symmetry

MDPI

*Article*

# Symmetry Classification of Antiferromagnets with Four Types of Multipoles

**Satoru Hayami**

Graduate School of Science, Hokkaido University, Sapporo 060-0810, Japan; hayami@phys.sci.hokudai.ac.jp

**Abstract:** A plethora of antiferromagnetic structures have been so far found in condensed matter physics, where the antiferromagnetic phase transition is characterized by symmetry lowering under the magnetic point group. Depending on the types of symmetry lowering, various cross-correlation phenomena, such as the anomalous Hall effect, magneto-electric effect, and magneto-piezoelectric effect, emerge below the critical temperature. We revisit a close relationship between the symmetry of the antiferromagnetic structures and cross-correlations based on the augmented multipoles consisting of electric, magnetic, magnetic toroidal, and electric toroidal multipoles with different spatial inversion and time-reversal parities. The symmetry classification will be useful for further exploration of functional antiferromagnetic materials.

**Keywords:** antiferromagnets; multipole; magnetic toroidal multipole; cross-correlation; magnetic point group; group theory

## 1. Introduction

Magnetic ordering is one of the most fundamental electronic orderings in solids, where the spin degree of freedom in electrons is ordered through the electron correlation. Owing to the breaking of time-reversal symmetry, various physical phenomena emerge below the magnetic phase transition temperature; ferromagnetic ordering gives rise to the anomalous Hall effect [1–7] and antiferromagnetic ordering breaking the spatial inversion symmetry gives rise to the linear magnetoelectric effect [8–14]. Meanwhile, recent studies have revealed that the same physical phenomena are often caused under totally different magnetic structures when the symmetry of the magnetic structures is the same. For example, the anomalous Hall effect is induced by various types of antiferromagnetic structures including collinear [15–22], noncollinear [23–27], and noncoplanar ones [28–31] when the symmetry of the antiferromagnetic state is the same as that of the ferromagnetic state. This example suggests that antiferromagnetic ordering has the potential to exhibit further intriguing physical phenomena, which would be important for the realization of functional antiferromagnetic materials applied to spintronic devices.

The concept of augmented multipoles has been introduced to smoothly make the antiferromagnetic structures correspond to physical phenomena [32,33]. There are four types of multipoles with different spatial inversion and time-reversal parities: electric multipole with $(\mathcal{P},\mathcal{T}) = [(-1)^l, +1]$, magnetic multipole with $(\mathcal{P},\mathcal{T}) = [(-1)^{l+1}, -1]$, magnetic toroidal multipole with $(\mathcal{P},\mathcal{T}) = [(-1)^l, -1]$, and electric toroidal multipole with $(\mathcal{P},\mathcal{T}) = [(-1)^{l+1}, +1]$, where $\mathcal{P}$ and $\mathcal{T}$ stand for the spatial inversion and time-reversal parities, respectively, and $l$ is the rank of the multipole. Since the four types of multipoles constitute a complete basis set in physical Hilbert space, any antiferromagnetic structures can be described by a ferroic alignment of any multipoles [34,35]. Figure 1 represents the examples of symmetry lowering by magnetic phase transitions under the tetragonal symmetry $4/mmm1'$; the antiferromagnetic structures are characterized by the magnetic monopole $M_0$ and the magnetic toroidal dipole $T_z$ with $(\mathcal{P},\mathcal{T}) = (-1,-1)$. Furthermore,

check for updates

**Citation:** Hayami, S. Symmetry Classification of Antiferromagnets with Four Types of Multipoles. *Symmetry* **2024**, *16*, 926. https://doi.org/10.3390/sym16070926

Academic Editors: Stefano Profumo and Alberto Ruiz Jimeno

Received: 15 June 2024
Revised: 13 July 2024
Accepted: 15 July 2024
Published: 19 July 2024

the systematic classification of antiferromagnetic structures has been performed under the 122 magnetic point groups based on magnetic representation analysis [36].

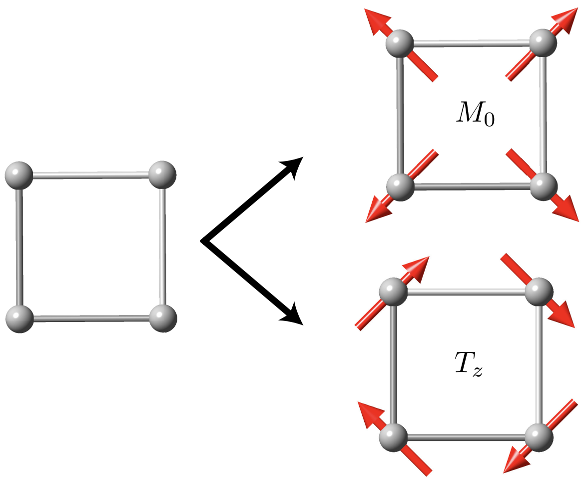


**Figure 1.** Examples of symmetry lowerings under magnetic phase transitions. The magnetic monopole ($M_0$) and the magnetic toroidal dipole ($T_z$) are induced when the $A_{1u}^-$ and $A_{2u}^-$ representations belong to the totally symmetric irreducible representation, where the superscript "−" of irrep indicates parity with respect to the antiunitary time-reversal operation.

In the present study, we revisit such a correspondence between antiferromagnetic structures and multipoles under 122 magnetic point groups in order to demonstrate which magnetic materials exhibit functional properties. By classifying the 122 magnetic point groups in terms of the four types of multipoles, we show that almost all of the magnetic point groups accompany the multipole moments up to rank 3, and hence, we expect rich cross-correlation phenomena in antiferromagnetic materials. In order to stimulate the experimental observation, we list candidate materials and expected cross-correlations in each multipole. The present results provide useful information not only in exploring functional antiferromagnetic materials but also in reexamining the well-known materials from the multipole viewpoint.

The rest of this paper is organized as follows: In Section 2, we first introduce the four types of multipoles. Then, we show the correspondence between antiferromagnetic structures and multipoles by taking an example in the tetragonal system in Section 3. In Section 4, we discuss the expected cross-correlations when the multipole is induced. We conclude the present results in Section 5.

## 2. Four Types of Multipoles

First, we briefly review the four types of multipoles, consisting of electric multipole $Q_{lm}$, magnetic multipole $M_{lm}$, magnetic toroidal multipole $T_{lm}$, and electric toroidal multipole $G_{lm}$, where the subscripts $l$ and $m$ represent the orbital angular momentum (rank of multipole) and its $z$ component, respectively; $m = -l, -l+1, \cdots, l$. The operator expressions of the four multipoles in spinless space are given by [37,38]

$$Q_{lm} = O_{lm}, \tag{1}$$

$$M_{lm} = \frac{1}{2}[(\boldsymbol{\nabla} O_{lm}) \cdot \hat{\boldsymbol{m}}_l + \hat{\boldsymbol{m}}_l \cdot (\boldsymbol{\nabla} O_{lm})], \tag{2}$$

$$T_{lm} = \frac{1}{2}\left[(\boldsymbol{\nabla} O_{lm}) \cdot \hat{\boldsymbol{t}} - \hat{\boldsymbol{t}} \cdot (\boldsymbol{\nabla} O_{lm})\right], \tag{3}$$

$$G_{lm} = \frac{1}{2}\left[(\nabla_\alpha \nabla_\beta O_{lm}) \hat{g}_l^{\alpha\beta} - (\hat{g}_l^{\alpha\beta})^\dagger (\nabla_\alpha \nabla_\beta O_{lm})\right], \tag{4}$$

where $O_{lm}(\boldsymbol{r})$ is proportional to the spherical harmonics as follows:

$$O_{lm}(\boldsymbol{r}) = \sqrt{\frac{4\pi}{2l+1}} r^l Y_{lm}(\hat{\boldsymbol{r}}), \tag{5}$$

with $\hat{\boldsymbol{r}} = \boldsymbol{r}/r$. $\hat{\boldsymbol{m}}_l$, $\hat{\boldsymbol{t}}_l$, and $\hat{g}_l^{\alpha\beta}$ are represented by

$$\hat{\boldsymbol{m}}_l = \frac{2\hat{\boldsymbol{l}}}{l+1}, \tag{6}$$

$$\hat{\boldsymbol{t}}_l = \frac{2}{(l+1)(l+2)}(\boldsymbol{r} \times \hat{\boldsymbol{l}}), \tag{7}$$

$$\hat{g}_l^{\alpha\beta} = \hat{t}_l^{\alpha} \hat{m}_l^{\beta}, \tag{8}$$

$$\hat{\boldsymbol{l}} = -i(\boldsymbol{r} \times \boldsymbol{\nabla}). \tag{9}$$

The expression of multipoles in spinful space is obtained by the addition rule of the above multipole operator and Pauli matrix in spin space [38].

We denote the monopole as $X_0$, dipole as $X_{1m} = (X_x, X_y, X_z)$, quadrupole as $X_{2m} = (X_u, X_v, X_{yz}, X_{zx}, X_{xy})$, and octupole as $X_{3m} = (X_{xyz}, X_x^{\alpha}, X_y^{\alpha}, X_z^{\alpha}, X_x^{\beta}, X_y^{\beta}, X_z^{\beta})$ for $X = Q, M, T, G$. The specific expressions of $O_{lm}$ up to rank 3 are given by

$$O_0 = 1, \tag{10}$$

$$(O_x, O_y, O_z) = (x, y, z), \tag{11}$$

$$O_u = \frac{1}{2}(3z^2 - r^2), \tag{12}$$

$$O_v = \frac{\sqrt{3}}{2}(x^2 - y^2), \tag{13}$$

$$(O_{yz}, O_{zx}, O_{xy}) = \sqrt{3}(yz, zx, xy), \tag{14}$$

$$O_{xyz} = \sqrt{15}xyz, \tag{15}$$

$$\left(O_x^{\alpha}, O_y^{\alpha}, O_z^{\alpha}\right) = \frac{1}{2}\left(x(5x^2 - 3r^2), y(5y^2 - 3r^2), z(5z^2 - 3r^2)\right), \tag{16}$$

$$\left(O_x^{\beta}, O_y^{\beta}, O_z^{\beta}\right) = \frac{\sqrt{15}}{2}\left(x(y^2 - z^2), y(z^2 - x^2), z(x^2 - y^2)\right). \tag{17}$$

The spatial inversion and time-reversal parities in each multipole are summarized in Table 1.

The four types of multipoles also describe the spin-split band structures and band deformations in momentum space. By reading $\boldsymbol{r}$ with the wave vector $\boldsymbol{k}$ in $O_{lm}(\boldsymbol{r})$, the momentum-space description of multipoles is given by [39]

$$Q_{lm}(\boldsymbol{k}) \equiv \begin{cases} \sigma_0 O_{lm}(\boldsymbol{k}) & (l = 0, 2, 4, 6, \cdots) \\ (\boldsymbol{k} \times \boldsymbol{\sigma}) \cdot \boldsymbol{\nabla}_{\boldsymbol{k}} O_{lm}(\boldsymbol{k}) & (l = 1, 3, 5, \cdots) \end{cases} \tag{18}$$

$$M_{lm}(\boldsymbol{k}) \equiv \begin{cases} 0 & (l = 0, 2, 4, 6, \cdots) \\ \boldsymbol{\sigma} \cdot \boldsymbol{\nabla}_{\boldsymbol{k}} O_{lm}(\boldsymbol{k}) & (l = 1, 3, 5, \cdots) \end{cases} \tag{19}$$

$$T_{lm}(\boldsymbol{k}) \equiv \begin{cases} 0 & (l = 0) \\ (\boldsymbol{k} \times \boldsymbol{\sigma}) \cdot \boldsymbol{\nabla}_{\boldsymbol{k}} O_{lm}(\boldsymbol{k}) & (l = 2, 4, 6, \cdots) \\ \sigma_0 O_{lm}(\boldsymbol{k}) & (l = 1, 3, 5, \cdots) \end{cases} \tag{20}$$

$$G_{lm}(\boldsymbol{k}) \equiv \begin{cases} \boldsymbol{k} \cdot \boldsymbol{\sigma} & (l = 0) \\ \boldsymbol{\sigma} \cdot \boldsymbol{\nabla}_{\boldsymbol{k}} O_{lm}(\boldsymbol{k}) & (l = 2, 4, 6, \cdots) \\ 0 & (l = 1, 3, 5, \cdots) \end{cases} \tag{21}$$

where $\sigma_0$ and $\boldsymbol{\sigma}$ denote the identity and Pauli matrices in spin space, respectively. Thus, the even-rank (odd-rank) electric (magnetic toroidal) multipoles describe the symmetric (antisymmetric) band deformation without spin dependence. Meanwhile, the odd-rank (even-rank) electric (magnetic toroidal) multipoles and the even-rank (odd-rank) electric toroidal (magnetic) multipoles describe the antisymmetric (symmetric) spin splitting in the band structure.

**Table 1.** Four types of multipoles (MPs) up to rank 3. "#" in the sixth column represents the number of magnetic point groups to possess multipoles in the totally symmetric irreducible representation. The seventh column represents the band dispersion in the presence of multipoles. The eighth, ninth, and tenth columns denote the induced multipoles under the electric field $\boldsymbol{E}$, magnetic field $\boldsymbol{H}$, and electric current $\boldsymbol{J}$.

| MP | Rank | Notation | $\mathcal{P}$ | $\mathcal{T}$ | # | Band Dispersion | $\boldsymbol{E}$ | $\boldsymbol{H}$ | $\boldsymbol{J}$ |
|---|---|---|---|---|---|---|---|---|---|
| E | 0 | $Q_0$ | +1 | +1 | 122 | 1 | $Q_{1m}$ | $M_{1m}$ | $T_{1m}$ |
| E | 1 | $Q_{1m}$ | −1 | +1 | 31 | $\boldsymbol{k}\times\boldsymbol{\sigma}$ | $Q_0, G_{1m}, Q_{2m}$ | $M_0, T_{1m}, M_{2m}$ | $T_0, M_{1m}, T_{2m}$ |
| E | 2 | $Q_{2m}$ | +1 | +1 | 106 | $O_{lm}(\boldsymbol{k})$ | $Q_{1m}, G_{2m}, Q_{3m}$ | $M_{1m}, T_{2m}, M_{3m}$ | $T_{1m}, M_{2m}, T_{3m}$ |
| E | 3 | $Q_{3m}$ | −1 | +1 | 58 | $(\boldsymbol{k}\times\boldsymbol{\sigma})\cdot\nabla_{\boldsymbol{k}}O_{lm}(\boldsymbol{k})$ | $Q_{2m}, G_{3m}, Q_{4m}$ | $M_{2m}, T_{3m}, M_{4m}$ | $T_{2m}, M_{3m}, T_{4m}$ |
| M | 0 | $M_0$ | −1 | −1 | 32 | – | $M_{1m}$ | $Q_{1m}$ | $G_{1m}$ |
| M | 1 | $M_{1m}$ | +1 | −1 | 31 | $\boldsymbol{\sigma}$ | $M_0, T_{1m}, M_{2m}$ | $Q_0, G_{1m}, Q_{2m}$ | $G_0, Q_{1m}, G_{2m}$ |
| M | 2 | $M_{2m}$ | −1 | −1 | 42 | – | $M_{1m}, T_{2m}, M_{3m}$ | $Q_{1m}, G_{2m}, Q_{3m}$ | $G_{1m}, Q_{2m}, G_{3m}$ |
| M | 3 | $M_{3m}$ | +1 | −1 | 58 | $\boldsymbol{\sigma}\cdot\nabla_{\boldsymbol{k}}O_{lm}(\boldsymbol{k})$ | $M_{2m}, T_{3m}, M_{4m}$ | $Q_{2m}, G_{3m}, Q_{4m}$ | $G_{2m}, Q_{3m}, G_{4m}$ |
| MT | 0 | $T_0$ | +1 | −1 | 32 | – | $T_{1m}$ | $G_{1m}$ | $Q_{1m}$ |
| MT | 1 | $T_{1m}$ | −1 | −1 | 31 | $\boldsymbol{k}$ | $T_0, M_{1m}, T_{2m}$ | $G_0, Q_{1m}, G_{2m}$ | $Q_0, G_{1m}, Q_{2m}$ |
| MT | 2 | $T_{2m}$ | +1 | −1 | 42 | $(\boldsymbol{k}\times\boldsymbol{\sigma})\cdot\nabla_{\boldsymbol{k}}O_{lm}(\boldsymbol{k})$ | $T_{1m}, M_{2m}, T_{3m}$ | $G_{1m}, Q_{2m}, G_{3m}$ | $Q_{1m}, G_{2m}, Q_{3m}$ |
| MT | 3 | $T_{3m}$ | −1 | −1 | 58 | $O_{lm}(\boldsymbol{k})$ | $T_{2m}, M_{3m}, T_{4m}$ | $G_{2m}, Q_{3m}, G_{4m}$ | $Q_{2m}, G_{3m}, Q_{4m}$ |
| ET | 0 | $G_0$ | −1 | +1 | 32 | $\boldsymbol{k}\cdot\boldsymbol{\sigma}$ | $G_{1m}$ | $T_{1m}$ | $M_{1m}$ |
| ET | 1 | $G_{1m}$ | +1 | +1 | 43 | – | $G_0, Q_{1m}, G_{2m}$ | $T_0, M_{1m}, T_{2m}$ | $M_0, T_{1m}, M_{2m}$ |
| ET | 2 | $G_{2m}$ | −1 | +1 | 42 | $\boldsymbol{\sigma}\cdot\nabla_{\boldsymbol{k}}O_{lm}(\boldsymbol{k})$ | $G_{1m}, Q_{2m}, G_{3m}$ | $T_{1m}, M_{2m}, T_{3m}$ | $M_{1m}, T_{2m}, M_{3m}$ |
| ET | 3 | $G_{3m}$ | +1 | +1 | 71 | – | $G_{2m}, Q_{3m}, G_{4m}$ | $T_{2m}, M_{3m}, T_{4m}$ | $M_{2m}, T_{3m}, M_{4m}$ |

The multipole description is also useful for understanding the cross-correlation phenomena when the external field or current is applied [39,40]. When the applied field/current is a rank-1 quantity, the rank of the induced multipoles is characterized by $l-1$, $l$, and $l+1$ for the rank-$l$ multipole in antiferromagnets. For example, when the electric field $\boldsymbol{E}$, which corresponds to $Q_{1m}$, is applied to the antiferromagnet with the magnetic toroidal dipole $T_{1m}$, any of the magnetic toroidal monopole $T_0$, magnetic dipole $M_{1m}$, or magnetic toroidal quadrupole $T_{2m}$ are induced depending on the field direction owing to the tensor product $Q_{1m}\otimes T_{1m}\to T_0\oplus M_{1m}\oplus T_{2m}$. Thus, the linear magneto-electric effect as a consequence of the cross-coupling between $M_{1m}$ and $Q_{1m}$ is expected under the $T_{1m}$ order. In addition, one finds that cross-correlations between $Q_{1m}$ and $T_0$ ($T_{2m}$) occur, which means that $T_0$ ($T_{2m}$) is induced by the electric field in antiferromagnets with $T_{1m}$. Similar cross-correlation phenomena are straightforwardly investigated for different fields/currents, such as the magnetic field $\boldsymbol{H}$ corresponding to $M_{1m}$ and the electric current $\boldsymbol{J}$ corresponding to $T_{1m}$. We summarize the correspondence among the multipoles, band dispersions, and couplings to $\boldsymbol{E}$, $\boldsymbol{H}$, and $\boldsymbol{J}$ in Table 1.

## 3. Multipoles in Antiferromagnets

By using the four types of multipoles, we describe any complicated magnetic structures by the ferroic alignment of the multipoles. In order to exemplify this, we consider the magnetic point group $4/mmm1'$. As shown in Table 2, all the irreducible representations without the time-reversal symmetry are characterized by either magnetic or magnetic toroidal multipoles [36]. For example, when the magnetic structure is characterized by the irreducible representation $\mathrm{B}_{1g}^{-}$, the magnetic toroidal quadrupole $T_v$ and magnetic octupole

$M_{xyz}$ are induced. In such a situation, one expects the appearance of the symmetric spin-split band structure and electric-field-induced magnetic quadrupole from Table 1.

The correspondence between the irreducible representations and magnetic patterns is investigated for the space group $P4/mmm$. We show the possible multipole orderings when the ions with the magnetic moments are located at the $1a$, $2f$, $4l$, and $8p$ sites in Table 2 [35]. For the $1a$ site, the possible magnetic structure is a ferromagnetic one, which indicates that only the irreducible representations corresponding to the magnetic dipole $(M_x, M_y, M_z)$ are possible. When the site symmetry is lowered, other multipoles belonging to different irreducible representations are induced; the magnetic toroidal quadrupole $T_{xy}$ belonging to the irreducible representation $\mathrm{B}_{2g}^-$ is possible for the $2f$ site and odd-parity multipoles like $M_0$ and $T_z$ are possible for the $4l$ site. Furthermore, in the case of the $8p$ site, all the irreducible representations are possible. The real-space spin configurations belonging to the different irreducible representations in the $8p$ site are shown in Figure 2. One finds that unconventional multipole orderings, such as the magnetic toroidal monopole $T_0$ belonging to $\mathrm{A}_{1g}^-$ and magnetic toroidal quadrupole $T_v$ belonging to $\mathrm{B}_{1g}^-$, are constructed various collinear and noncollinear spin configurations.

**Table 2.** Irreducible representations (irreps) of four types of multipoles under the magnetic point group (MPG) $4/mmm1'$ [36]. The superscript "$-$" of irrep indicates the parity with respect to the antiunitary time-reversal operation. MP in the second column represents the multipole, which corresponds to the order parameter under magnetic orderings. From the fourth to seventh columns, possible $\boldsymbol{q} = \mathbf{0}$ magnetic orderings for the Wyckoff positions under the space group $P4/mmm$ are shown [35].

| Irrep | MP | Subgroup | $1a$ (0 0 0) | $2f$ (0 1/2 0) | $4l$ ($x$ 0 0) | $8p$ ($x$ $y$ 0) |
|---|---|---|---|---|---|---|
| $\mathrm{A}_{1g}^-$ | $T_0, T_u$ | $4/mmm$ | – | – | – | ✓ |
| $\mathrm{A}_{2g}^-$ | $M_z, M_z^\alpha$ | $4/mm'm'$ | ✓ | ✓ | ✓ | ✓ |
| $\mathrm{B}_{1g}^-$ | $T_v, M_{xyz}$ | $4'/mmm'$ | – | – | – | ✓ |
| $\mathrm{B}_{2g}^-$ | $T_{xy}, M_z^\beta$ | $4'/mm'm$ | – | ✓ | ✓ | ✓ |
| $\mathrm{E}_g^-$ | $T_{yz}, M_x, M_x^\alpha, M_x^\beta$ | $mm'm'$ | ✓ | ✓ | ✓ | ✓ |
| | $T_{zx}, M_y, M_y^\alpha, M_y^\beta$ | $m'mm'$ | ✓ | ✓ | ✓ | ✓ |
| $\mathrm{A}_{1u}^-$ | $M_0, M_u$ | $4/m'm'm'$ | – | – | ✓ | ✓ |
| $\mathrm{A}_{2u}^-$ | $T_z, T_z^\alpha$ | $4/m'mm$ | – | – | ✓ | ✓ |
| $\mathrm{B}_{1u}^-$ | $T_{xyz}, M_v$ | $4'/m'm'm$ | – | – | ✓ | ✓ |
| $\mathrm{B}_{2u}^-$ | $T_z^\beta, M_{xy}$ | $4'/m'mm'$ | – | – | ✓ | ✓ |
| $\mathrm{E}_u^-$ | $T_x, T_x^\alpha, T_x^\beta, M_{yz}$ | $m'mm$ | – | – | ✓ | ✓ |
| | $T_y, T_y^\alpha, T_y^\beta, M_{zx}$ | $mm'm$ | – | – | ✓ | ✓ |

The above example indicates that various multipoles are activated in the antiferromagnetic structures according to their magnetic point groups. Indeed, 32, 31, 42, and 58 out of 122 magnetic point groups possess $M_0$, $M_{1m}$, $M_{2m}$, and $M_{3m}$, respectively. Similarly, 122, 31, 106, and 58 magnetic point groups possess $Q_0$, $Q_{1m}$, $Q_{2m}$, and $Q_{3m}$, respectively, 32, 31, 42, and 58 magnetic point groups possess $T_0$, $T_{1m}$, $T_{2m}$, and $T_{3m}$, respectively, and 32, 43, 42, and 71 magnetic point groups possess $G_0$, $G_{1m}$, $G_{2m}$, and $G_{3m}$, respectively. In order to show the active multipoles under 122 magnetic point groups, we classify them in each magnetic point group, as shown in Table 3. It is noted that magnetic structures without the breaking of the time-reversal symmetry are possible when the $\boldsymbol{q} \neq \mathbf{0}$ state is considered. The typical magnetic materials from MAGNDATA [41] are also listed. This table is useful for seeing which types of multipoles are present in magnetic materials.

**Table 3.** Classification of four types of multipoles up to rank 3 under the 122 magnetic point groups. The number in the column for the multipoles $X_{lm}$ $(X = Q, M, T, G)$ represents the number of active multipoles belonging to the totally symmetric irreducible representation. The materials taken from MAGNDATA [41] are also listed in the rightmost column.

| | | $(\mathcal{P}, \mathcal{T}) = (+1, +1)$ | | | | $(-1, +1)$ | | | | $(+1, -1)$ | | | | $(-1, -1)$ | | | | |
|---|---|---|---|---|---|---|---|---|---|---|---|---|---|---|---|---|---|---|
| | **MPG** | $Q_0$ | $Q_{2m}$ | $G_{1m}$ | $G_{3m}$ | $G_0$ | $G_{2m}$ | $Q_{1m}$ | $Q_{3m}$ | $T_0$ | $T_{2m}$ | $M_{1m}$ | $M_{3m}$ | $M_0$ | $M_{2m}$ | $T_{1m}$ | $T_{3m}$ | **Material** |
| #1 | $1$ | 1 | 5 | 3 | 7 | 1 | 5 | 3 | 7 | 1 | 5 | 3 | 7 | 1 | 5 | 3 | 7 | $Mn_2ScSbO_6$ [42] |
| #2 | $11'$ | 1 | 5 | 3 | 7 | 1 | 5 | 3 | 7 | | | | | | | | | $LiFeAs_2O_7$ [43] |
| #3 | $\bar{1}$ | 1 | 5 | 3 | 7 | | | | | 1 | 5 | 3 | 7 | | | | | $RbMnF_4$ [44] |
| #4 | $\bar{1}1'$ | 1 | 5 | 3 | 7 | | | | | | | | | | | | | $CuMnO_2$ [45] |
| #5 | $\bar{1}'$ | 1 | 5 | 3 | 7 | | | | | | | | | 1 | 5 | 3 | 7 | $MnPSe_3$ [46] |
| #6 | $2$ | 1 | 3 | 1 | 3 | 1 | 3 | 1 | 3 | 1 | 3 | 1 | 3 | 1 | 3 | 1 | 3 | $LiFeP_2O_7$ [47] |
| #7 | $21'$ | 1 | 3 | 1 | 3 | 1 | 3 | 1 | 3 | | | | | | | | | $Yb_2CoMnO_6$ [48] |
| #8 | $2'$ | 1 | 3 | 1 | 3 | 1 | 3 | 1 | 3 | | 2 | 2 | 4 | | 2 | 2 | 4 | $BaDy_2O_4$ [49] |
| #9 | $m$ | 1 | 3 | 1 | 3 | | 2 | 2 | 4 | 1 | 3 | 1 | 3 | | 2 | 2 | 4 | $Mn_4Nb_2O_9$ [50] |
| #10 | $m1'$ | 1 | 3 | 1 | 3 | | 2 | 2 | 4 | | | | | | | | | $DyFeWO_6$ [51] |
| #11 | $m'$ | 1 | 3 | 1 | 3 | | 2 | 2 | 4 | | 2 | 2 | 4 | 1 | 3 | 1 | 3 | $ScFeO_3$ [52] |
| #12 | $2/m$ | 1 | 3 | 1 | 3 | | | | | 1 | 3 | 1 | 3 | | | | | $Cu_2OSO_4$ [53] |
| #13 | $2/m1'$ | 1 | 3 | 1 | 3 | | | | | | | | | | | | | $CuSe_2O_5$ [54] |
| #14 | $2'/m$ | 1 | 3 | 1 | 3 | | | | | | | | | | 2 | 2 | 4 | $YbCl_3$ [55] |
| #15 | $2/m'$ | 1 | 3 | 1 | 3 | | | | | | | | | 1 | 3 | 1 | 3 | $Co_2V_2O_7$ [56] |
| #16 | $2'/m'$ | 1 | 3 | 1 | 3 | | | | | | 2 | 2 | 4 | | | | | $Mn_3Ti_2Te_6$ [57] |
| #17 | $222$ | 1 | 2 | | 1 | 1 | 2 | | 1 | 1 | 2 | | 1 | 1 | 2 | | 1 | $FePO_4$ [58] |
| #18 | $2221'$ | 1 | 2 | | 1 | 1 | 2 | | 1 | | | | | | | | | $AgNiO_2$ [59] |
| #19 | $2'2'2$ | 1 | 2 | | 1 | 1 | 2 | | 1 | | 1 | 1 | 2 | | 1 | 1 | 2 | $VNb_3S_6$ [60] |
| #20 | $mm2$ | 1 | 2 | | 1 | | 1 | 1 | 2 | 1 | 2 | | 1 | | 1 | 1 | 2 | $FeSb_2O_4$ [61] |
| #21 | $mm21'$ | 1 | 2 | | 1 | | 1 | 1 | 2 | | | | | | | | | $EuNiO_3$ [62] |
| #22 | $m'm2'$ | 1 | 2 | | 1 | | 1 | 1 | 2 | | 1 | 1 | 2 | | 1 | 1 | 2 | $CaBaCo_4O_7$ [63] |
| #23 | $m'm'2$ | 1 | 2 | | 1 | | 1 | 1 | 2 | | 1 | 1 | 2 | 1 | 2 | | 1 | $\alpha$-$Cu_2V_2O_7$ [64] |
| #24 | $mmm$ | 1 | 2 | | 1 | | | | | 1 | 2 | | 1 | | | | | $\alpha$-$Mn_2O_3$ [65] |
| #25 | $mmm1'$ | 1 | 2 | | 1 | | | | | | | | | | | | | $BaFe_2As_2$ [66] |
| #26 | $mmm'$ | 1 | 2 | | 1 | | | | | | | | | | 1 | 1 | 2 | $U_3Ru_4Al_{12}$ [67] |
| #27 | $m'm'm$ | 1 | 2 | | 1 | | | | | | 1 | 1 | 2 | | | | | $NiF_2$ [68] |
| #28 | $m'm'm'$ | 1 | 2 | | 1 | | | | | | | | | 1 | 2 | | 1 | $TbB_4$ [69] |
| #29 | $4$ | 1 | 1 | 1 | 1 | 1 | 1 | 1 | 1 | 1 | 1 | 1 | 1 | 1 | 1 | 1 | 1 | $Ce_5TeO_8$ [70] |
| #30 | $41'$ | 1 | 1 | 1 | 1 | 1 | 1 | 1 | 1 | | | | | | | | | $CeAuAl_3$ [71] |

**Table 3.** *Cont.*

| | MPG | $(\mathcal{P}, \mathcal{T}) = (+1, +1)$ | | | | $(-1, +1)$ | | | | $(+1, -1)$ | | | | $(-1, -1)$ | | | | Material |
|---|---|---|---|---|---|---|---|---|---|---|---|---|---|---|---|---|---|---|
| | | $Q_0$ | $Q_{2m}$ | $G_{1m}$ | $G_{3m}$ | $G_0$ | $G_{2m}$ | $Q_{1m}$ | $Q_{3m}$ | $T_0$ | $T_{2m}$ | $M_{1m}$ | $M_{3m}$ | $M_0$ | $M_{2m}$ | $T_{1m}$ | $T_{3m}$ | |
| #31 | $4'$ | 1 | 1 | 1 | 1 | 1 | 1 | 1 | 1 | | 2 | | 2 | | 2 | | 2 | |
| #32 | $\bar{4}$ | 1 | 1 | 1 | 1 | | 2 | | 2 | 1 | 1 | 1 | 1 | | 2 | | 2 | |
| #33 | $\bar{4}1'$ | 1 | 1 | 1 | 1 | | 2 | | 2 | | | | | | | | | |
| #34 | $\bar{4}'$ | 1 | 1 | 1 | 1 | | 2 | | 2 | | 2 | | 2 | 1 | 1 | 1 | 1 | $CsCoF_4$ [72] |
| #35 | $4/m$ | 1 | 1 | 1 | 1 | | | | | 1 | 1 | 1 | 1 | | | | | $Mn_3CuN$ [73] |
| #36 | $4/m1'$ | 1 | 1 | 1 | 1 | | | | | | | | | | | | | $Sr_2FeOsO_6$ [74] |
| #37 | $4'/m$ | 1 | 1 | 1 | 1 | | | | | | 2 | | 2 | | | | | |
| #38 | $4/m'$ | 1 | 1 | 1 | 1 | | | | | | | | | 1 | 1 | 1 | 1 | $TlFe_{1.6}Se_2$ [75] |
| #39 | $4'/m'$ | 1 | 1 | 1 | 1 | | | | | | | | | | 2 | | 2 | $KOsO_4$ [76] |
| #40 | $422$ | 1 | 1 | | | 1 | 1 | | | 1 | 1 | | | 1 | 1 | | | $Ho_2Ge_2O_7$ [77] |
| #41 | $4221'$ | 1 | 1 | | | 1 | 1 | | | | | | | | | | | $Ba(TiO)Cu_4(PO_4)_4$ [78] |
| #42 | $4'22'$ | 1 | 1 | | | 1 | 1 | | | | 1 | | 1 | | 1 | | 1 | $Er_2Ge_2O_7$ [79] |
| #43 | $42'2'$ | 1 | 1 | | | 1 | 1 | | | | | 1 | 1 | | | 1 | 1 | $Nd_5Si_4$ [80] |
| #44 | $4mm$ | 1 | 1 | | | | | 1 | 1 | 1 | 1 | | | | | 1 | 1 | |
| #45 | $4mm1'$ | 1 | 1 | | | | | 1 | 1 | | | | | | | | | $CeRhGe_3$ [81] |
| #46 | $4'mm'$ | 1 | 1 | | | | | 1 | 1 | | 1 | | 1 | | 1 | | 1 | |
| #47 | $4m'm'$ | 1 | 1 | | | | | 1 | 1 | | | 1 | 1 | 1 | 1 | | | $CeIrGe_3$ [82] |
| #48 | $\bar{4}2m$ | 1 | 1 | | | | 1 | | 1 | 1 | 1 | | | | 1 | | 1 | $Ba_2MnSi_2O_7$ [83] |
| #49 | $\bar{4}2m1'$ | 1 | 1 | | | | 1 | | 1 | | | | | | | | | $GeCu_2O_4$ [84] |
| #50 | $\bar{4}'m2'$ | 1 | 1 | | | | 1 | | 1 | | 1 | | 1 | | | 1 | 1 | |
| #51 | $\bar{4}'2m'$ | 1 | 1 | | | | 1 | | 1 | | 1 | | 1 | 1 | 1 | | | $Ce_4Sb_3$ [85] |
| #52 | $\bar{4}2'm'$ | 1 | 1 | | | | 1 | | 1 | | | 1 | 1 | | 1 | | 1 | $EuCr_2As_2$ [86] |
| #53 | $4/mmm$ | 1 | 1 | | | | | | | 1 | 1 | | | | | | | $CdYb_2S_4$ [87] |
| #54 | $4/mmm1'$ | 1 | 1 | | | | | | | | | | | | | | | $EuMn_2Si_2$ [88] |
| #55 | $4/m'mm$ | 1 | 1 | | | | | | | | | | | | | 1 | 1 | $Co_3Al_2Si_3O_{12}$ [89] |
| #56 | $4'/mmm'$ | 1 | 1 | | | | | | | | 1 | | 1 | | | | | $CoF_2$ [90] |
| #57 | $4'/m'm'm$ | 1 | 1 | | | | | | | | | | | | 1 | | 1 | $BaMn_2Bi_2$ [91] |
| #58 | $4/mm'm'$ | 1 | 1 | | | | | | | | | 1 | 1 | | | | | $Ho_2Ru_2O_7$ [92] |
| #59 | $4/m'm'm'$ | 1 | 1 | | | | | | | | | | | 1 | 1 | | | $GdB_4$ [93] |
| #60 | $3$ | 1 | 1 | 1 | 3 | 1 | 1 | 1 | 3 | 1 | 1 | 1 | 3 | 1 | 1 | 1 | 3 | $Cu_2OSeO_3$ [94] |
| #61 | $31'$ | 1 | 1 | 1 | 3 | 1 | 1 | 1 | 3 | | | | | | | | | $RbFe(MoO_4)_2$ [95] |
| #62 | $\bar{3}$ | 1 | 1 | 1 | 3 | | | | | 1 | 1 | 1 | 3 | | | | | $NiN_2O_6$ [96] |
| #63 | $\bar{3}1'$ | 1 | 1 | 1 | 3 | | | | | | | | | | | | | $LaMn_3V_4O_{12}$ [97] |
| #64 | $\bar{3}'$ | 1 | 1 | 1 | 3 | | | | | | | | | 1 | 1 | 1 | 3 | $MgMnO_3$ [98] |
| #65 | $32$ | 1 | 1 | | 1 | 1 | 1 | | 1 | 1 | 1 | | 1 | 1 | 1 | | 1 | $La_{0.33}Sr_{0.67}FeO_3$ [99] |

**Table 3.** *Cont.*

| | MPG | $(\mathcal{P},\mathcal{T})=(+1,+1)$ | | | | $(-1,+1)$ | | | | $(+1,-1)$ | | | | $(-1,-1)$ | | | | Material |
|---|---|---|---|---|---|---|---|---|---|---|---|---|---|---|---|---|---|---|
| | | $Q_0$ | $Q_{2m}$ | $G_{1m}$ | $G_{3m}$ | $G_0$ | $G_{2m}$ | $Q_{1m}$ | $Q_{3m}$ | $T_0$ | $T_{2m}$ | $M_{1m}$ | $M_{3m}$ | $M_0$ | $M_{2m}$ | $T_{1m}$ | $T_{3m}$ | |
| #66 | $321'$ | 1 | 1 | | 1 | 1 | 1 | | 1 | | | | | | | | | $DyFe_3(BO_3)_4$ [100] |
| #67 | $32'$ | 1 | 1 | | 1 | 1 | 1 | | 1 | | | 1 | 1 | | | 1 | 1 | $BaCu_3V_2O_8(OD)_2$ [101] |
| #68 | $3m$ | 1 | 1 | | 1 | | | 1 | 1 | 1 | 1 | | 1 | | | 1 | 1 | $PbNiO_3$ [102] |
| #69 | $3m1'$ | 1 | 1 | | 1 | | | 1 | 1 | | | | | | | | | $Ba_3Nb_2NiO_9$ [103] |
| #70 | $3m'$ | 1 | 1 | | 1 | | | 1 | 1 | | | 1 | 1 | 1 | 1 | | 1 | CrSe [104] |
| #71 | $\bar{3}m$ | 1 | 1 | | 1 | | | | | 1 | 1 | | 1 | | | | | $Li_2MnTeO_6$ [105] |
| #72 | $\bar{3}m1'$ | 1 | 1 | | 1 | | | | | | | | | | | | | $SrRu_2O_6$ [106] |
| #73 | $\bar{3}'m$ | 1 | 1 | | 1 | | | | | | | | | | | 1 | 2 | $Ca_2YZr_2Fe_3O_{12}$ [107] |
| #74 | $\bar{3}'m'$ | 1 | 1 | | 1 | | | | | | | | | 1 | 1 | | 1 | $Na_2MnTeO_6$ [108] |
| #75 | $\bar{3}m'$ | 1 | 1 | | 1 | | | | | | | 1 | 2 | | | | | $Co_3Sn_2S_2$ [109] |
| #76 | $6$ | 1 | 1 | 1 | 1 | 1 | 1 | 1 | 1 | 1 | 1 | 1 | 1 | 1 | 1 | 1 | 1 | $BaCoSiO_4$ [110] |
| #77 | $61'$ | 1 | 1 | 1 | 1 | 1 | 1 | 1 | 1 | | | | | | | | | |
| #78 | $6'$ | 1 | 1 | 1 | 1 | 1 | 1 | 1 | 1 | | | | 1 | | | | 1 | $YMnO_3$ [111] |
| #79 | $\bar{6}$ | 1 | 1 | 1 | 1 | | | | 1 | 1 | 1 | 1 | 1 | | | | 1 | |
| #80 | $\bar{6}1'$ | 1 | 1 | 1 | 1 | | | | 1 | | | | | | | | | ErAuIn [112] |
| #81 | $\bar{6}'$ | 1 | 1 | 1 | 1 | | | | 1 | | | | 1 | 1 | 1 | 1 | 1 | $Tb_{14}Ag_{51}$ [113] |
| #82 | $6/m$ | 1 | 1 | 1 | 1 | | | | | 1 | 1 | 1 | 1 | | | | | $FeF_3$ [114] |
| #83 | $6/m1'$ | 1 | 1 | 1 | 1 | | | | | | | | | | | | | |
| #84 | $6'/m$ | 1 | 1 | 1 | 1 | | | | | | | | | | | | 2 | $K_2Mn_3(VO_4)_2CO_3$ [115] |
| #85 | $6/m'$ | 1 | 1 | 1 | 1 | | | | | | | | | 1 | 1 | 1 | 1 | $U_{14}Au_{51}$ [116] |
| #86 | $6'/m'$ | 1 | 1 | 1 | 1 | | | | | | | | 2 | | | | | |
| #87 | $622$ | 1 | 1 | | | 1 | 1 | | | 1 | 1 | | | 1 | 1 | | | |
| #88 | $6221'$ | 1 | 1 | | | 1 | 1 | | | | | | | | | | | $ScMn_6Ge_6$ [117] |
| #89 | $6'22'$ | 1 | 1 | | | 1 | 1 | | | | | | 1 | | | | 1 | |
| #90 | $62'2'$ | 1 | 1 | | | 1 | 1 | | | | | 1 | 1 | | | 1 | 1 | $EuIn_2As_2$ [118] |
| #91 | $6mm$ | 1 | 1 | | | | | 1 | 1 | 1 | 1 | | | | | 1 | 1 | $HoMnO_3$ [119] |
| #92 | $6mm1'$ | 1 | 1 | | | | | 1 | 1 | | | | | | | | | |
| #93 | $6'mm'$ | 1 | 1 | | | | | 1 | 1 | | | | 1 | | | | 1 | $Co_2Mo_3O_8$ [120] |
| #94 | $6m'm'$ | 1 | 1 | | | | | 1 | 1 | | | 1 | 1 | 1 | 1 | | | $LuFeO_3$ [121] |
| #95 | $\bar{6}m2$ | 1 | 1 | | | | | | 1 | 1 | 1 | | | | | | 1 | $Ba_3CoSb_2O_9$ [122] |
| #96 | $\bar{6}m21'$ | 1 | 1 | | | | | | 1 | | | | | | | | | $CsCr_{0.94}Fe_{0.06}F_4$ [123] |
| #97 | $\bar{6}'m'2$ | 1 | 1 | | | | | | 1 | | | | 1 | 1 | 1 | | | UNiGa [124] |
| #98 | $\bar{6}'m2'$ | 1 | 1 | | | | | | 1 | | | | 1 | | | 1 | 1 | $CsFeCl_3$ [125] |
| #99 | $\bar{6}m'2'$ | 1 | 1 | | | | | | 1 | | | 1 | 1 | | | | 1 | HoPdIn [126] |
| #100 | $6/mmm$ | 1 | 1 | | | | | | | 1 | 1 | | | | | | | |

**Table 3.** *Cont.*

| | | $(\mathcal{P},\mathcal{T})=(+1,+1)$ | | | | $(-1,+1)$ | | | | $(+1,-1)$ | | | | $(-1,-1)$ | | | | |
|---|---|---|---|---|---|---|---|---|---|---|---|---|---|---|---|---|---|---|
| | **MPG** | $Q_0$ | $Q_{2m}$ | $G_{1m}$ | $G_{3m}$ | $G_0$ | $G_{2m}$ | $Q_{1m}$ | $Q_{3m}$ | $T_0$ | $T_{2m}$ | $M_{1m}$ | $M_{3m}$ | $M_0$ | $M_{2m}$ | $T_{1m}$ | $T_{3m}$ | **Material** |
| #101 | $6/mmm1'$ | 1 | 1 | | | | | | | | | | | | | | | FeGe [127] |
| #102 | $6/m'mm$ | 1 | 1 | | | | | | | | | | | | | 1 | 1 | |
| #103 | $6'/mmm'$ | 1 | 1 | | | | | | | | | | | | | | 1 | |
| #104 | $6'/m'mm'$ | 1 | 1 | | | | | | | | | | 1 | | | | | $CsCoCl_3$ [128] |
| #105 | $6/mm'm'$ | 1 | 1 | | | | | | | | | 1 | 1 | | | | | $Fe_{2.71}GeTe_2$ [129] |
| #106 | $6/m'm'm'$ | 1 | 1 | | | | | | | | | | | 1 | 1 | | | |
| #107 | $23$ | 1 | | | 1 | 1 | | | 1 | 1 | | | 1 | 1 | | | 1 | $Mn_3IrSi$ [130] |
| #108 | $231'$ | 1 | | | 1 | 1 | | | 1 | | | | | | | | | MnGe [131] |
| #109 | $m\bar{3}$ | 1 | | | 1 | | | | | 1 | | | 1 | | | | | $MnTe_2$ [132] |
| #110 | $m\bar{3}1'$ | 1 | | | 1 | | | | | | | | | | | | | $Au_{72}Al_{14}Tb_{14}$ [133] |
| #111 | $m'\bar{3}'$ | 1 | | | 1 | | | | | | | | | 1 | | | 1 | |
| #112 | $432$ | 1 | | | | 1 | | | | 1 | | | | 1 | | | | $SrCuTe_2O_6$ [134] |
| #113 | $4321'$ | 1 | | | | 1 | | | | | | | | | | | | |
| #114 | $4'32'$ | 1 | | | | 1 | | | | | | | 1 | | | | 1 | $BaCuTe_2O_6$ [135] |
| #115 | $\bar{4}3m$ | 1 | | | | | | | 1 | 1 | | | | | | | 1 | |
| #116 | $\bar{4}3m1'$ | 1 | | | | | | | 1 | | | | | | | | | $Gd_2Ti_2O_7$ [136] |
| #117 | $\bar{4}'3m'$ | 1 | | | | | | | 1 | | | | 1 | 1 | | | | |
| #118 | $m\bar{3}m$ | 1 | | | | | | | | 1 | | | | | | | | |
| #119 | $m\bar{3}m1'$ | 1 | | | | | | | | | | | | | | | | NdZn [137] |
| #120 | $m'\bar{3}'m$ | 1 | | | | | | | | | | | | | | | 1 | |
| #121 | $m\bar{3}m'$ | 1 | | | | | | | | | | | 1 | | | | | $Tb_3Ga_5O_{12}$ [138] |
| #122 | $m'\bar{3}'m'$ | 1 | | | | | | | | | | | | 1 | | | | |

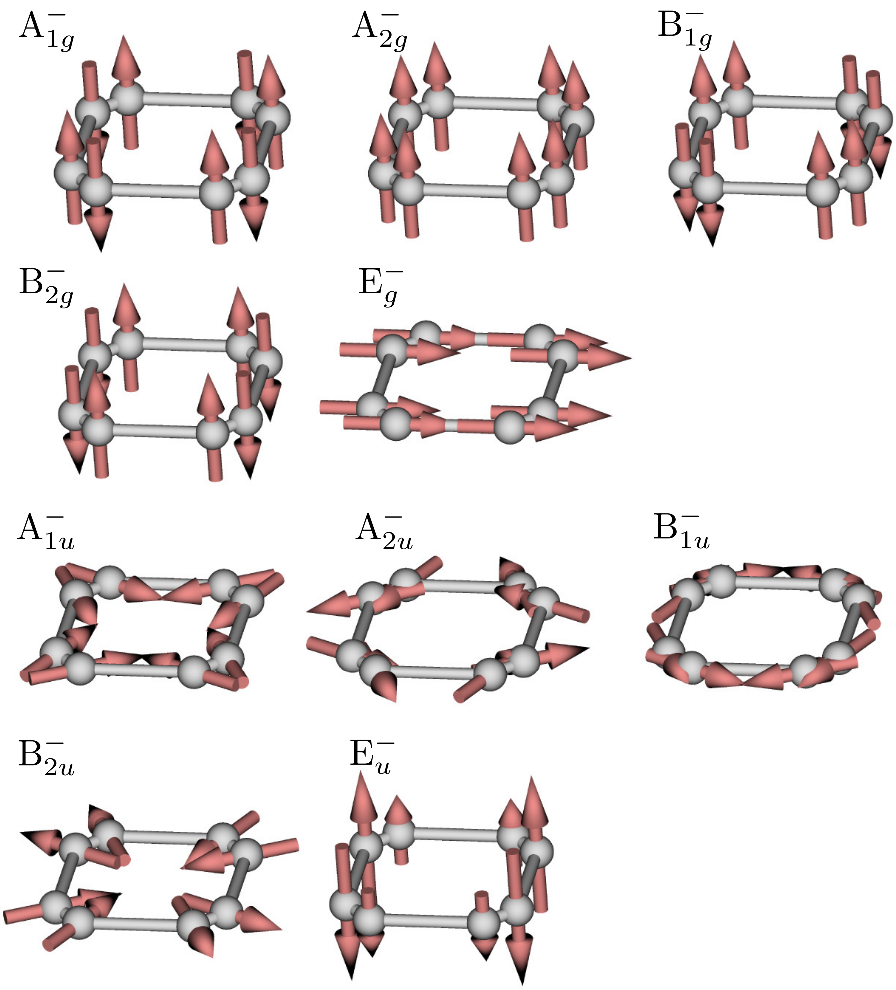


**Figure 2.** Magnetic structures belonging to different irreducible representations for the $8p$ site under the space group $P4/mmm$. The arrows represent the direction of magnetic moments.

## 4. Cross-Correlations in Antiferromagnets with Multipoles

In this section, we briefly show the expected cross-correlations and transports in magnetic materials with multipoles: the electric dipole $Q_{1m}$ in Section 4.1, the electric quadrupole $Q_{2m}$ in Section 4.2, the electric octupole $Q_{3m}$ in Section 4.3, the magnetic monopole $M_0$ in Section 4.4, the magnetic dipole $M_{1m}$ in Section 4.5, the magnetic quadrupole $M_{2m}$ in Section 4.6, the magnetic octupole $M_{3m}$ in Section 4.7, the magnetic toroidal monopole $T_0$ in Section 4.8, the magnetic toroidal dipole $T_{1m}$ in Section 4.9, the magnetic toroidal quadrupole $T_{2m}$ in Section 4.10, the magnetic toroidal octupole $T_{3m}$ in Section 4.11, the electric toroidal monopole $G_0$ in Section 4.12, the electric toroidal dipole $G_{1m}$ in Section 4.13, the electric toroidal quadrupole $G_{2m}$ in Section 4.14, and the electric toroidal octupole $G_{3m}$ in Section 4.15.

### 4.1. Electric Dipole

There are 31 magnetic point groups accompanying the electric dipole $Q_{1m}$, as shown in Table 4. We classify 31 magnetic point groups in terms of the presence and absence of $M_{1m}$ and $T_{1m}$. Since $M_{1m}$ and $T_{1m}$ are coupled to the magnetic field and electric current, respectively, they can be used to control the domain of the antiferromagnetic state with $Q_{1m}$.

**Table 4.** Classification of magnetic point groups (MPGs) with the electric dipole $Q_{1m}$ according to the presence and absence of the magnetic dipole $M_{1m}$ and the magnetic toroidal dipole $T_{1m}$.

| MPG | $M_{1m}$ | $T_{1m}$ |
|---|---|---|
| $1, 2, 2', m, m', m'm2', 4, 3, 6$ | ✓ | ✓ |
| $m'm'2, 4m'm', 3m', 6m'm'$ | ✓ | |
| $mm2, 4mm, 3m, 6mm$ | | ✓ |
| $11', 21', m1', mm21', 41', 4', 4mm1'$ | | |
| $4'mm', 31', 3m1', 61', 6', 6mm1', 6'mm'$ | | |

The magnetic materials with $Q_{1m}$ exhibit the antisymmetric spin polarization in the band structure, which corresponds to the Rashba-type spin–orbit coupling in the form of $\boldsymbol{k} \times \boldsymbol{\sigma}$. Accordingly, the transverse Edelstein effect, where the magnetization is induced by the electric current in a perpendicular way, occurs. The materials with $Q_{1m}$ also show the nonlinear Hall effect based on the Berry curvature dipole mechanism [139]. Moreover, the system with $Q_{1m}$ shows the magnetic toroidal moment in the external magnetic field. One of the candidate materials is CrSe, where the symmetry reduces from $P6_3/mmc$ to $P31m'$ (magnetic point group $3m'$) by the magnetic phase transition [104]. In this material, the above physical phenomena are induced only below the critical temperature. In addition, the single domain can be obtained by performing magnetic field cooling.

### *4.2. Electric Quadrupole*

There are 106 magnetic point groups accompanying the electric quadrupole $Q_{2m}$. We classify them in terms of the presence and absence of $Q_{1m}$, $M_{1m}$, and $T_{1m}$, as shown in Table 5, where the presence of $Q_{1m}$ means that the single-domain formation can be controlled by applying the electric field when $Q_{1m}$ is simultaneously induced below the critical temperature. The nematic ordering belongs to this category.

**Table 5.** Classification of magnetic point groups (MPGs) with the electric quadrupole $Q_{2m}$ according to the presence and absence of the electric dipole $Q_{1m}$, the magnetic dipole $M_{1m}$, and the magnetic toroidal dipole $T_{1m}$.

| MPG | $Q_{1m}$ | $M_{1m}$ | $T_{1m}$ |
|---|---|---|---|
| $1, 2, 2', m, m', m'm2', 4, 3, 6$ | ✓ | ✓ | ✓ |
| $m'm'2, 4m'm', 3m', 6m'm'$ | ✓ | ✓ | |
| $mm2, 4mm, 3m, 6mm$ | ✓ | | ✓ |
| $2'2'2, 42'2', 32', 62'2'$ | | ✓ | ✓ |
| $11', 21', m1', mm21', 41', 4', 4mm1'$ | ✓ | | |
| $4'mm', 31', 3m1', 61', 6', 6mm1', 6'mm'$ | ✓ | | |
| $\bar{1}, 2/m, 2'/m', m'm'm, \bar{4}, 4/m, \bar{4}2'm'$ | | ✓ | |
| $4/mm'm', \bar{3}, \bar{3}m', \bar{6}, 6/m, \bar{6}m'2', 6/mm'm'$ | | ✓ | |
| $\bar{1}', 2'/m, 2/m', mmm', \bar{4}', 4/m', \bar{4}'m2'$ | | | ✓ |
| $4/m'mm, \bar{3}', \bar{3}'m, \bar{6}', 6/m', \bar{6}'m2', 6/m'mm$ | | | ✓ |
| $\bar{1}1', 2/m1', 222, 2221', mmm, mmm1', m'm'm'$ | | | |
| $\bar{4}1', 4/m1', 4'/m, 4'/m', 422, 4221', 4'22', \bar{4}2m$ | | | |
| $\bar{4}2m1', \bar{4}'2m', 4/mmm, 4/mmm1', 4'/mmm'$ | | | |
| $4'/m'm'm, 4/m'm'm', \bar{3}1', 32, 321', \bar{3}m$ | | | |
| $\bar{3}m1', \bar{3}'m', \bar{6}1', 6/m1', 6'/m, 6'/m', 622$ | | | |
| $6221', 6'22', \bar{6}m2, \bar{6}m21', \bar{6}'m'2, 6/mmm$ | | | |
| $6/mmm1', 6'/mmm', 6'/m'mm', 6/m'm'm'$ | | | |

Although $Q_{2m}$ has the same spatial inversion and time-reversal properties as the electric monopole $Q_0$, it exhibits intriguing electromagnetic responses according to its spatial anisotropy. In addition to the conjugate physical quantities, additional higher-rank multipoles are induced under external fields and currents. In other words, the responses against the fields and currents are different from the case with $Q_0$. For example, the electric toroidal quadrupole $G_{2m}$, the magnetic toroidal quadrupole $T_{2m}$, and the magnetic quadrupole $M_{2m}$ are induced by the electric field, magnetic field, and electric current, respectively. In particular, the momentum-dependent spin splitting, which arises from $T_{2m}$, in addition to Zeeman-type uniform spin splitting, occurs in the magnetic field.

### 4.3. Electric Octupole

The electric octupole $Q_{3m}$ is included in 58 magnetic point groups, where 27 magnetic point groups do not possess $Q_{1m}$, as shown in Table 6. Similarly to $Q_{1m}$, the magnetic materials with $Q_{3m}$ also exhibit the antisymmetric spin-split band structure including the Dresselhaus-type one in the form of $k_x(k_y^2 - k_z^2)\sigma_x + k_y(k_z^2 - k_x^2)\sigma_y + k_z(k_x^2 - k_y^2)\sigma_z$. Meanwhile, the magnetic octupole instead of the magnetic dipole (magnetization) is induced by the electric current in contrast to $Q_{1m}$. The candidate material is $VNb_3S_6$, where the symmetry reduction occurs from $P6_322$ to $C2'2'2_1$ (magnetic point group $2'2'2$) [60]. Since $M_{1m}$ and $T_{1m}$ are simultaneously induced under $2'2'2$, either the magnetic field or electric current cooling can lead to the single domain of $Q_{3m}$.

**Table 6.** Classification of magnetic point groups (MPGs) with the electric octupole $Q_{3m}$ according to the presence and absence of the electric dipole $Q_{1m}$, the magnetic dipole $M_{1m}$, and the magnetic toroidal dipole $T_{1m}$. The upper (lower) columns represent the magnetic point groups with (without) $Q_{1m}$.

| MPG | $Q_{1m}$ | $M_{1m}$ | $T_{1m}$ |
|---|---|---|---|
| $1, 2, 2', m, m', m'm2', 4, 3, 6$ | ✓ | ✓ | ✓ |
| $m'm'2, 4m'm', 3m', 6m'm'$ | ✓ | ✓ | |
| $mm2, 4mm, 3m, 6mm$ | ✓ | | ✓ |
| $11', 21', m1', mm21', 41', 4', 4mm1'$ | ✓ | | |
| $4'mm', 31', 3m1', 61', 6', 6mm1', 6'mm'$ | ✓ | | |
| $2'2'2, 32'$ | | ✓ | ✓ |
| $\bar{4}, \bar{4}2'm', \bar{6}, \bar{6}m'2'$ | | ✓ | |
| $\bar{4}', \bar{4}'m2', \bar{6}', \bar{6}'m2'$ | | | ✓ |
| $222, 2221', \bar{4}1', \bar{4}2m, \bar{4}2m1', \bar{4}'2m'$ | | | |
| $32, 321', \bar{6}1', \bar{6}m2, \bar{6}m21', \bar{6}'m'2$ | | | |
| $23, 231', \bar{4}3m, \bar{4}3m1', \bar{4}'3m'$ | | | |

### 4.4. Magnetic Monopole

Among 122 magnetic point groups, 32 magnetic point groups include the magnetic monopole $M_0$, as shown in Table 7. This becomes the origin of the linear longitudinal magneto-electric effect, where the magnetization $M_{1m}$ (electric polarization $Q_{1m}$) is induced in the electric-field (magnetic-field) direction [140–143]. $TbB_4$ (magnetic point group $m'm'm'$) [69,144,145] and $FePO_4$ (magnetic point group 222) [58] are typical examples to exhibit physical phenomena related to magnetic monopoles.

**Table 7.** Classification of magnetic point groups (MPGs) with the magnetic monopole $M_0$ according to the presence and absence of the electric dipole $Q_{1m}$, the magnetic dipole $M_{1m}$, and the magnetic toroidal dipole $T_{1m}$.

| MPG | $Q_{1m}$ | $M_{1m}$ | $T_{1m}$ |
|---|---|---|---|
| $1, 2, m', 4, 3, 6$ | ✓ | ✓ | ✓ |
| $m'm'2, 4m'm', 3m', 6m'm'$ | ✓ | ✓ | |
| $\bar{1}', 2/m', \bar{4}', 4/m', \bar{3}', \bar{6}', 6/m'$ | | | ✓ |
| $222, m'm'm', 422, \bar{4}'2m', 4/m'm'm', 32, \bar{3}'m'$ | | | |
| $622, \bar{6}'m'2, 6/m'm'm', 23, m'\bar{3}', 432, \bar{4}'3m', m'\bar{3}'m'$ | | | |

### 4.5. Magnetic Dipole

The magnetic dipole $M_{1m}$ is included in 31 magnetic point groups, as shown in Table 8 [146–148]. Since $M_{1m}$ corresponds to the ferroic alignment of spin, i.e., the ferromagnetic state, the Berry curvature occurs in the band structure, which becomes the origin of the physical phenomena under magnetization or magnetic field occur, such as the Hall effect, Nernst effect, and magneto-optical Kerr effect [149,150]. Meanwhile, the magnetic point groups with $M_{1m}$ are also realized in the antiferromagnetic structure even without (or with a negligibly small) net magnetization, as found in the noncollinear antiferromagnets like $Mn_3Sn$ [25,26,151–153] and collinear antiferromagnets [19,154] like La$MO_3$ ($M =$ Cr, Mn, and Fe) [15], the bilayer $MnPSe_3$ [16], $\kappa$-type organic conductors [18], and so on. Recently, different types of magnetic dipole have been introduced such as the "anisotropic magnetic dipole" $M'_{1m}$, which consists of the product of the electric quadrupole $Q_{2m}$ and conventional magnetic dipole (spin) $M_{1m}$, and they are regarded as a microscopic indicator of the presence of the anomalous Hall effect in antiferromagnets [21,155]. Since the symmetry conditions for $M_{1m}$ and $M'_{1m}$ are the same as each other, the magnetic materials belonging to 31 magnetic point groups in Table 8 result in "ferromagnetic" physical phenomena irrespective of the ferromagnetic and antiferromagnetic structures.

**Table 8.** Classification of magnetic point groups (MPGs) with the magnetic dipole $M_{1m}$ according to the presence and absence of the electric dipole $Q_{1m}$ and the magnetic toroidal dipole $T_{1m}$.

| MPG | $Q_{1m}$ | $T_{1m}$ |
|---|---|---|
| $1, 2, 2', m, m', m'm2', 4, 3, 6$ | ✓ | ✓ |
| $m'm'2, 4m'm', 3m', 6m'm'$ | ✓ | |
| $2'2'2, 42'2', 32', 62'2'$ | | ✓ |
| $\bar{1}, 2/m, 2'/m', m'm'm, \bar{4}, 4/m, \bar{4}2'm'$ | | |
| $4/mm'm', \bar{3}, \bar{3}m', \bar{6}, 6/m, \bar{6}m'2', 6/mm'm'$ | | |

In addition, the materials with $M_{1m}$ exhibit further cross-correlations. One of the examples is the switching response between the magnetic dipole and magnetic toroidal dipole ($T_{1m}$) of circularly polarized light. Another example is the electric-current-induced chirality (electric toroidal monopole $G_0$).

### 4.6. Magnetic Quadrupole

A total of 42 out of 122 magnetic point groups possess the magnetic quadrupole $M_{2m}$, as shown in Table 9; of these, 27 magnetic point groups accompany $M_0$, while the remaining 15 magnetic point groups do not have $M_0$. Since the physical properties of $M_{2m}$ are similar to those of $M_0$ owing to the same spatial inversion and time-reversal parities, it is desired to focus on the materials listed in the lower columns when the pure nature of the magnetic quadrupole is investigated. Similarly to the materials with $M_0$, the materials with $M_{2m}$ show the linear magneto-electric effect [156–158], as found in $Cr_2O_3$ [159–163]. In addition, $M_{2m}$ becomes the microscopic origin of the magneto-piezoelectric effect found in EuMnBi [164,165], which arises from the spin-orbital-momentum locking in the band structure [166], and the intrinsic nonlinear Hall effect [167–169]. $KOsO_4$ (magnetic point group $4'/m'$) [76,170] and $Er_2Ge_2O_7$ (magnetic point group $4'22'$) [79] are other candidate materials with $M_{2m}$ but without $Q_{1m}$, $M_{1m}$, or $T_{1m}$.

**Table 9.** Classification of magnetic point groups (MPGs) with the magnetic quadrupole $M_{2m}$ according to the presence and absence of the electric dipole $Q_{1m}$, the magnetic dipole $M_{1m}$, the magnetic toroidal dipole $T_{1m}$, and the magnetic monopole $M_0$. The upper (lower) columns represent the magnetic point groups with (without) $M_0$.

| MPG | $Q_{1m}$ | $M_{1m}$ | $T_{1m}$ | $M_0$ |
|---|---|---|---|---|
| $1, 2, m', 4, 3, 6$ | ✓ | ✓ | ✓ | ✓ |
| $m'm'2, 4m'm', 3m', 6m'm'$ | ✓ | ✓ | | ✓ |
| $\bar{1}', 2/m', \bar{4}', 4/m', \bar{3}', \bar{6}', 6/m'$ | | | ✓ | ✓ |
| $222, m'm'm', 422, \bar{4}'2m', 4/m'm'm'$ | | | | ✓ |
| $32, \bar{3}'m', 622, \bar{6}'m'2, 6/m'm'm'$ | | | | ✓ |
| $2', m, m'm2'$ | ✓ | ✓ | ✓ | |
| $mm2$ | ✓ | | ✓ | |
| $2'2'2$ | | ✓ | ✓ | |
| $4', 4'mm'$ | ✓ | | | |
| $\bar{4}, \bar{4}2'm'$ | | ✓ | | |
| $2'/m, mmm'$ | | | ✓ | |
| $4'/m', 4'22', \bar{4}2m, 4'/m'm'm$ | | | | |

## 4.7. Magnetic Octupole

There are 58 magnetic point groups to possess the magnetic octupole $M_{3m}$, as shown in Table 10. Among them, 27 magnetic point groups are characterized by the magnetic point groups without $M_{1m}$; the pure effect of $M_{3m}$ is expected. The materials with magnetic octupole $M_{3m}$ induce rank-2, rank-3, and rank-4 multipoles when external fields and currents are applied. Since $T_{3m}$ ($Q_{2m}$) are induced for the applied electric field (magnetic field), the band structure is modulated in an antisymmetric (symmetric) way. In addition, $M_{3m}$ becomes the microscopic origin of the magnetic-field-induced striction, i.e., magnetostriction [171]. $Er_2Ge_2O_7$ (magnetic point group $4'22'$) [79] is one of the candidates to have $M_{3m}$.

**Table 10.** Classification of magnetic point groups (MPGs) with the magnetic octupole $M_{3m}$ according to the presence and absence of the electric dipole $Q_{1m}$, the magnetic dipole $M_{1m}$, and the magnetic toroidal dipole $T_{1m}$. The upper (lower) columns represent the magnetic point groups with (without) $M_{1m}$.

| MPG | $Q_{1m}$ | $M_{1m}$ | $T_{1m}$ |
|---|---|---|---|
| $1, 2, 2', m, m', m'm2', 4, 3, 6$ | ✓ | ✓ | ✓ |
| $m'm'2, 4m'm', 3m', 6m'm'$ | ✓ | ✓ | |
| $2'2'2, 42'2', 32', 62'2'$ | | ✓ | ✓ |
| $\bar{1}, 2/m, 2'/m', m'm'm, \bar{4}, 4/m, \bar{4}2'm'$ | | ✓ | |
| $4/mm'm', \bar{3}, \bar{3}m', \bar{6}, 6/m, \bar{6}m'2', 6/mm'm'$ | | ✓ | |
| $mm2, 3m$ | ✓ | | ✓ |
| $4', 4'mm', 6', 6'mm'$ | ✓ | | |
| $\bar{4}', \bar{4}'m2', \bar{6}', \bar{6}'m2'$ | | | ✓ |
| $222, mmm, 4'/m, 4'22', \bar{4}'2m', 4'/mmm'$ | | | |
| $32, \bar{3}m, 6'/m', 6'22', \bar{6}'m'2, 6'/m'mm'$ | | | |
| $23, m\bar{3}, 4'32', \bar{4}'3m', m\bar{3}m'$ | | | |

## 4.8. Magnetic Toroidal Monopole

Magnetic toroidal monopole $T_0$ is included in the 32 magnetic point groups, as shown in Table 11. Since $T_0$ corresponds to a time-reversal-odd scalar quantity, it leads to the time-reversal switching responses, such as the electric-field-induced magnetic toroidal dipole $T_{1m}$ and the magnetic-field-induced electric toroidal dipole $G_{1m}$ [172,173]. Such cross-correlations have recently been observed in $Co_2SiO_4$ [174]. Another candidate is $Ho_2Ge_2O_7$ under magnetic point group 422 [77], for example.

**Table 11.** Classification of magnetic point groups (MPGs) with the magnetic toroidal monopole $T_0$ according to the presence and absence of the electric dipole $Q_{1m}$, the magnetic dipole $M_{1m}$, and the magnetic toroidal dipole $T_{1m}$.

| MPG | $Q_{1m}$ | $M_{1m}$ | $T_{1m}$ |
|---|---|---|---|
| $1, 2, m, 4, 3, 6$ | ✓ | ✓ | ✓ |
| $mm2, 4mm, 3m, 6mm$ | ✓ | | ✓ |
| $\bar{1}, 2/m, \bar{4}, 4/m, \bar{3}, \bar{6}, 6/m$ | | ✓ | |
| $222, mmm, 422, \bar{4}2m, 4/mmm, 32, \bar{3}m, 622$ | | | |
| $\bar{6}m2, 6/mmm, 23, m\bar{3}, 432, \bar{4}3m, m\bar{3}m$ | | | |

*4.9. Magnetic Toroidal Dipole*

Magnetic toroidal dipole $T_{1m}$ is allowed for 31 magnetic point groups, as shown in Table 12 [175]. It is the most typical multipole degree of freedom to exhibit the cross-correlation phenomena in magnetic materials. The representative phenomenon is the linear transverse magneto-electric effect in magnetic insulators [176–180], although a similar phenomenon has been observed in magnetic metals like $UNi_4B$ [181–185]. In addition, as $T_{1m}$ corresponds to the time-reversal-odd polar vector, it gives rise to asymmetric band deformation without the spin dependence. Accordingly, $T_{1m}$ induces further cross-correlations and transports, such as nonreciprocal transport [186–190], asymmetric magnon excitations [191–193], and nonlinear spin Hall/Nernst effect [194,195].

**Table 12.** Classification of magnetic point groups (MPGs) with the magnetic toroidal dipole $T_{1m}$ according to the presence and absence of the electric dipole $Q_{1m}$ and the magnetic dipole $M_{1m}$.

| MPG | $Q_{1m}$ | $M_{1m}$ |
|---|---|---|
| $1, 2, 2', m, m', m'm2', 4, 3, 6$ | ✓ | ✓ |
| $mm2, 4mm, 3m, 6mm$ | ✓ | |
| $2'2'2, 42'2', 32', 62'2'$ | | ✓ |
| $\bar{1}', 2'/m, 2/m', mmm', \bar{4}', 4/m', \bar{4}'m2'$ | | |
| $4/m'mm, \bar{3}', \bar{3}'m, \bar{6}', 6/m', \bar{6}'m2', 6/m'mm$ | | |

*4.10. Magnetic Toroidal Quadrupole*

There are 42 magnetic point groups to possess the magnetic toroidal quadrupole $T_{2m}$, as shown in Table 13; 27 out of 42 magnetic point groups possess $T_0$, whereas 15 magnetic point groups do not. The materials with $T_{2m}$ show the momentum-dependent symmetric spin-split band structure, which results in the directional-dependent spin current generation [196,197]. Moreover, in the materials with $T_{2m}$, the ferroaxial nature is induced when the magnetic field is applied. One of the candidate materials is $CoF_2$ under magnetic point group $4'/mmm'$ [90], although the domain control might be difficult in this material owing to no simple conjugate fields to $T_{2m}$. In this context, $Mn_3Ti_2Te_6$ under magnetic point group $2'/m'$ [57] is another candidate material, where the magnetic field cooling enables us to select a single domain.

**Table 13.** Classification of magnetic point groups (MPGs) with the magnetic toroidal quadrupole $T_{2m}$ according to the presence and absence of the electric dipole $Q_{1m}$, the magnetic dipole $M_{1m}$, the magnetic toroidal dipole $T_{1m}$, and the magnetic toroidal monopole $T_0$. The upper (lower) columns represent the magnetic point groups with (without) $T_0$.

| MPG | $Q_{1m}$ | $M_{1m}$ | $T_{1m}$ | $T_0$ |
|---|---|---|---|---|
| $1, 2, m, 4, 3, 6$ | ✓ | ✓ | ✓ | ✓ |
| $mm2, 4mm, 3m, 6mm$ | ✓ | | ✓ | ✓ |
| $\bar{1}, 2/m, \bar{4}, 4/m, \bar{3}, \bar{6}, 6/m$ | | ✓ | | ✓ |
| $222, mmm, 422, \bar{4}2m, 4/mmm, 32$ | | | | ✓ |
| $\bar{3}m, 622, \bar{6}m2, 6/mmm$ | | | | ✓ |
| $2', m', m'm2'$ | ✓ | ✓ | ✓ | |
| $m'm'2$ | ✓ | ✓ | | |
| $2'2'2$ | | ✓ | ✓ | |
| $4', 4'mm'$ | ✓ | | | |
| $2'/m', m'm'm$ | | ✓ | | |
| $\bar{4}', \bar{4}'m2'$ | | | ✓ | |
| $4'/m, 4'22', \bar{4}'2m', 4'/mmm'$ | | | | |

*4.11. Magnetic Toroidal Octupole*

A total of 58 magnetic point groups possess the magnetic toroidal octupole $T_{3m}$, where 31 magnetic point groups also possess $T_{1m}$, as shown in Table 14. Since $T_{3m}$ induces asymmetric band modulation similar to $T_{1m}$, the materials with $T_{3m}$ show nonreciprocal transport against the electric field and thermal gradient [198–200]. One of the potential candidates is CrSe under the magnetic point group $3m'$ [104], where physical phenomena related to the MT octupole can be controlled by both electric and magnetic fields.

**Table 14.** Classification of magnetic point groups (MPGs) with the magnetic toroidal octupole $T_{3m}$ according to the presence and absence of the electric dipole $Q_{1m}$, the magnetic dipole $M_{1m}$, and the magnetic toroidal dipole $T_{1m}$. The upper (lower) columns represent the magnetic point groups with (without) $T_{1m}$.

| MPG | $Q_{1m}$ | $M_{1m}$ | $T_{1m}$ |
|---|---|---|---|
| $1, 2, 2', m, m', m'm2', 4, 3, 6$ | ✓ | ✓ | ✓ |
| $mm2, 4mm, 3m, 6mm$ | ✓ | | ✓ |
| $2'2'2, 42'2', 32', 62'2'$ | | ✓ | ✓ |
| $\bar{1}', 2'/m, 2/m', mmm', \bar{4}', 4/m', \bar{4}'m2'$ | | | ✓ |
| $4/m'mm, \bar{3}', \bar{3}'m, \bar{6}', 6/m', \bar{6}'m2', 6/m'mm$ | | | ✓ |
| $m'm'2, 3m'$ | ✓ | ✓ | |
| $4', 4'mm', 6', 6'mm'$ | ✓ | | |
| $\bar{4}, \bar{4}2'm', \bar{6}, \bar{6}m'2'$ | | ✓ | |
| $222, m'm'm', 4'/m', 4'22', \bar{4}2m, 4'/m'm'm$ | | | |
| $32, \bar{3}'m', 6'/m, 6'22', \bar{6}m2$ | | | |
| $6'/mmm', 23, m'\bar{3}', 4'32', \bar{4}3m, m'\bar{3}'m$ | | | |

*4.12. Electric Toroidal Monopole*

A total of 32 magnetic point groups possess the electric toroidal monopole $G_0$, as shown in Table 15. As $G_0$ is characterized as the time-reversal-even pseudoscalar quantity, it corresponds to the chirality [201–203], which becomes the microscopic origin of the hedgehog-type antisymmetric spin–orbit coupling $\boldsymbol{k} \cdot \boldsymbol{\sigma}$, the longitudinal Edelstein effect [204–206], and the electrical magnetochiral effect [207]. Although such a chirality is usually accompanied by lattice structures without the mirror and spatial inversion symmetries, it can be generated by the magnetic phase transition when $G_0$ additionally belongs to the totally symmetric irreducible representation below the critical temperature. For example, $FePO_4$ under magnetic point group 222 [58], $ScMn_6Ge_6$ under magnetic point group $6221'$ [117], and $La_{0.33}Sr_{0.67}FeO_3$ under magnetic point group 32 [99] belong to the materials showing the $G_0$ property driven by the magnetic phase transition.

**Table 15.** Classification of magnetic point groups (MPGs) with the electric toroidal monopole $G_0$ according to the presence and absence of the electric dipole $Q_{1m}$, the magnetic dipole $M_{1m}$, and the magnetic toroidal dipole $T_{1m}$.

| MPG | $Q_{1m}$ | $M_{1m}$ | $T_{1m}$ |
|---|---|---|---|
| $1, 2, 2', 4, 3, 6$ | ✓ | ✓ | ✓ |
| $2'2'2, 42'2', 32', 62'2'$ | | ✓ | ✓ |
| $11', 21', 41', 4', 31', 61', 6'$ | ✓ | | |
| $222, 2221', 422, 4221', 4'22', 32, 321', 622$ | | | |
| $6221', 6'22', 23, 231', 432, 4321', 4'32'$ | | | |

### 4.13. Electric Toroidal Dipole

The electric toroidal dipole $G_{1m}$ is included in 43 magnetic point groups, as shown in Table 16. The electric toroidal dipole has recently been attracted since it brings about an unconventional electronic state, invariant under both spatial inversion and time-reversal operations; its ordering is referred to as ferro-rotational order or ferro-axial order [208–212], which have been observed in $RbFe(MoO_4)_2$ [210,213] and $NiTiO_3$ [213–216]. The materials with $G_{1m}$ exhibit transverse responses of the conjugate physical quantities, such as antisymmetric thermopolarization [217], longitudinal spin current generation [218,219], nonlinear transverse magnetization [220], and second-order nonlinear magnetostriction [221]. Such physical properties driven by $G_{1m}$ can be induced by the magnetic phase transition. $FeF_3$, which undergoes the phase transition from $P6/mmm$ to $P6_3/m$ (magnetic point group $6/m$), is one of the candidate materials to exhibit the property of $G_{1m}$ by magnetic phase transition [114]. Another candidate is a magnetic vortex accompanying both magnetic monopole and magnetic toroidal dipole [222]. In magnetic materials, $G_{1m}$ contributes to the magnetic anisotropy to tilt the spin moments from the crystal axis by combining the relativistic spin–orbit coupling [223].

**Table 16.** Classification of magnetic point groups (MPGs) with the electric toroidal dipole $G_{1m}$ according to the presence and absence of the electric dipole $Q_{1m}$, the magnetic dipole $M_{1m}$, and the magnetic toroidal dipole $T_{1m}$.

| MPG | $Q_{1m}$ | $M_{1m}$ | $T_{1m}$ |
|---|---|---|---|
| $1, 2, 2', m, m', 4, 3, 6$ | ✓ | ✓ | ✓ |
| $11', 21', m1', 41', 4', 31', 61', 6'$ | ✓ | | |
| $\bar{1}, 2/m, 2'/m', \bar{4}, 4/m, \bar{3}, \bar{6}, 6/m$ | | ✓ | |
| $\bar{1}', 2'/m, 2/m', \bar{4}', 4/m', \bar{3}', \bar{6}', 6/m'$ | | | ✓ |
| $\bar{1}1', 2/m1', \bar{4}1', 4/m1', 4'/m, 4'/m'$ | | | |
| $\bar{3}1', \bar{6}1', 6/m1', 6'/m, 6'/m'$ | | | |

### 4.14. Electric Toroidal Quadrupole

The electric toroidal quadrupole $G_{2m}$ can be found in 42 magnetic point groups, as shown in Table 17. Among them, 27 magnetic point groups also possess $G_0$. The materials with $G_{2m}$ show parity-violating physical phenomena, such as the nonlinear Hall effect based on the Berry curvature dipole mechanism [139] and Edelstein effect [224–226]. $GeCu_2O_4$ under the magnetic point group $\bar{4}2m1'$ is one of the candidate materials to exhibit the physical phenomena of $G_{2m}$ below the critical temperature [84].

**Table 17.** Classification of magnetic point groups (MPGs) with the electric toroidal quadrupole $G_{2m}$ according to the presence and absence of the electric dipole $Q_{1m}$, the magnetic dipole $M_{1m}$, the magnetic toroidal dipole $T_{1m}$, and the electric toroidal monopole $G_0$. The upper (lower) columns represent the magnetic point groups with (without) $G_0$.

| MPG | $Q_{1m}$ | $M_{1m}$ | $T_{1m}$ | $G_0$ |
|---|---|---|---|---|
| $1, 2, 2', 4, 3, 6$ | ✓ | ✓ | ✓ | ✓ |
| $2'2'2, 42'2', 32', 62'2'$ | | ✓ | ✓ | ✓ |
| $11', 21', 41', 4', 31', 61', 6'$ | ✓ | | | ✓ |
| $222, 2221', 422, 4221', 4'22'$ | | | | ✓ |
| $32, 321', 622, 6221', 6'22'$ | | | | ✓ |
| $m, m', m'm2'$ | ✓ | ✓ | ✓ | |
| $m'm'2$ | ✓ | ✓ | | |
| $mm2$ | ✓ | | ✓ | |
| $m1', mm21'$ | ✓ | | | |
| $\bar{4}, \bar{4}2'm'$ | | ✓ | | |
| $\bar{4}', \bar{4}'m2'$ | | | ✓ | |
| $\bar{4}1', \bar{4}2m, \bar{4}2m1', \bar{4}'2m'$ | | | | |

### 4.15. Electric Toroidal Octupole

There are 71 magnetic point groups that include the electric toroidal octupole $G_{3m}$, as shown in Table 18. Of these, 28 out of the 71 do not possess $G_{1m}$. Although the physical phenomena of $G_{3m}$ have not been investigated compared to other multipoles, the materials with $G_{3m}$ show similar physical phenomena to $G_{1m}$ owing to the same spatial inversion and time-reversal parities. For example, the longitudinal spin current generation is possible in materials with $G_{3m}$ [219]. $FePO_4$ (magnetic point group 222) [58] is one of the candidates to exhibit physical phenomena by $G_{3m}$ through the magnetic phase transition.

**Table 18.** Classification of magnetic point groups (MPGs) with the electric toroidal octupole $G_{3m}$ according to the presence and absence of the electric dipole $Q_{1m}$, the magnetic dipole $M_{1m}$, the magnetic toroidal dipole $T_{1m}$, and the electric toroidal dipole $G_{1m}$. The upper (lower) columns represent the magnetic point groups with (without) $G_{1m}$.

| MPG | $Q_{1m}$ | $M_{1m}$ | $T_{1m}$ | $G_{1m}$ |
|---|---|---|---|---|
| $1, 2, 2', m, m', 4, 3, 6$ | ✓ | ✓ | ✓ | ✓ |
| $11', 21', m1', 41', 4', 31', 61', 6'$ | ✓ | | | ✓ |
| $\bar{1}, 2/m, 2'/m', \bar{4}, 4/m, \bar{3}, \bar{6}, 6/m$ | | ✓ | | ✓ |
| $\bar{1}', 2'/m, 2/m', \bar{4}', 4/m', \bar{3}', \bar{6}', 6/m'$ | | | ✓ | ✓ |
| $\bar{1}1', 2/m1', \bar{4}1', 4/m1', 4'/m, 4'/m'$ | | | | ✓ |
| $\bar{3}1', \bar{6}1', 6/m1', 6'/m, 6'/m'$ | | | | ✓ |
| $m'm2'$ | ✓ | ✓ | ✓ | |
| $m'm'2, 3m'$ | ✓ | ✓ | | |
| $mm2, 3m$ | ✓ | | ✓ | |
| $2'2'2, 32'$ | | ✓ | ✓ | |
| $mm21', 3m1'$ | ✓ | | | |
| $m'm'm, \bar{3}m'$ | | ✓ | | |
| $mmm', \bar{3}'m$ | | | ✓ | |
| $222, 2221', mmm, mmm1', m'm'm', 32, 321'$ | | | | |
| $\bar{3}m, \bar{3}m1', \bar{3}'m', 23, 231', m\bar{3}, m\bar{3}1', m'\bar{3}'$ | | | | |

## 5. Conclusions

To summarize, we have revisited the multipole classification under 122 magnetic point groups, with an emphasis on magnetic materials. We have shown that four types of multipoles (electric, magnetic, magnetic toroidal, and electric toroidal multipoles) emerge in magnetic materials irrespective of their rank. Since each multipole gives rise to different cross-correlations and transports, the systematic correspondence between multipoles and magnetic point groups enables us to design and engineer functional magnetic materials, including topological spin textures like magnetic skyrmions [227–229], which will be useful for future spintronic applications.

**Funding:** This research was supported by JSPS KAKENHI Grants Numbers JP21H01037, JP22H00101, JP22H01183, JP23H04869, JP23K03288, JP23K20827, and by JST CREST (JPMJCR23O4).

**Data Availability Statement:** The data presented in this study are available on request from the corresponding author.

**Conflicts of Interest:** The author declares no conflicts of interest.

## References

1. Karplus, R.; Luttinger, J.M. Hall Effect in Ferromagnetics. *Phys. Rev.* **1954**, *95*, 1154–1160. [CrossRef]
2. Smit, J. The spontaneous Hall effect in ferromagnetics II. *Physica* **1958**, *24*, 39–51. [CrossRef]
3. Maranzana, F.E. Contributions to the Theory of the Anomalous Hall Effect in Ferro- and Antiferromagnetic Materials. *Phys. Rev.* **1967**, *160*, 421–429. [CrossRef]
4. Berger, L. Side-Jump Mechanism for the Hall Effect of Ferromagnets. *Phys. Rev. B* **1970**, *2*, 4559–4566. [CrossRef]
5. Nozieres, P.; Lewiner, C. A simple theory of the anomalous Hall effect in semiconductors. *J. Phys.* **1973**, *34*, 901–915. [CrossRef]
6. Jungwirth, T.; Niu, Q.; MacDonald, A.H. Anomalous Hall Effect in Ferromagnetic Semiconductors. *Phys. Rev. Lett.* **2002**, *88*, 207208. [CrossRef]
7. Gosálbez-Martínez, D.; Souza, I.; Vanderbilt, D. Chiral degeneracies and Fermi-surface Chern numbers in bcc Fe. *Phys. Rev. B* **2015**, *92*, 085138. [CrossRef]
8. Kimura, T.; Goto, T.; Shintani, H.; Ishizaka, K.; Arima, T.; Tokura, Y. Magnetic control of ferroelectric polarization. *Nature* **2003**, *426*, 55–58. [CrossRef] [PubMed]
9. Fiebig, M. Revival of the magnetoelectric effect. *J. Phys. D Appl. Phys.* **2005**, *38*, R123. [CrossRef]
10. Spaldin, N.A.; Fiebig, M. The renaissance of magnetoelectric multiferroics. *Science* **2005**, *309*, 391–392. [CrossRef] [PubMed]
11. Ramesh, R.; Spaldin, N.A. Multiferroics: Progress and prospects in thin films. *Nat. Mater.* **2007**, *6*, 21. [CrossRef] [PubMed]
12. Khomskii, D. Classifying multiferroics: Mechanisms and effects. *Physics* **2009**, *2*, 20. [CrossRef]
13. Tokura, Y.; Seki, S.; Nagaosa, N. Multiferroics of spin origin. *Rep. Prog. Phys.* **2014**, *77*, 076501. [CrossRef] [PubMed]
14. Fiebig, M.; Lottermoser, T.; Meier, D.; Trassin, M. The evolution of multiferroics. *Nat. Rev. Mater.* **2016**, *1*, 16046. [CrossRef]
15. Solovyev, I.V. Magneto-optical effect in the weak ferromagnets $LaMO_3$ (M = Cr, Mn, and Fe). *Phys. Rev. B* **1997**, *55*, 8060–8063. [CrossRef]
16. Sivadas, N.; Okamoto, S.; Xiao, D. Gate-Controllable Magneto-optic Kerr Effect in Layered Collinear Antiferromagnets. *Phys. Rev. Lett.* **2016**, *117*, 267203. [CrossRef]
17. Li, X.; MacDonald, A.H.; Chen, H. Quantum Anomalous Hall Effect through Canted Antiferromagnetism. *arXiv* **2019**, arXiv:1902.10650.
18. Naka, M.; Hayami, S.; Kusunose, H.; Yanagi, Y.; Motome, Y.; Seo, H. Anomalous Hall effect in $\kappa$-type organic antiferromagnets. *Phys. Rev. B* **2020**, *102*, 075112. [CrossRef]
19. Šmejkal, L.; González-Hernández, R.; Jungwirth, T.; Sinova, J. Crystal time-reversal symmetry breaking and spontaneous Hall effect in collinear antiferromagnets. *Sci. Adv.* **2020**, *6*, eaaz8809. [CrossRef] [PubMed]
20. Samanta, K.; Ležaić, M.; Merte, M.; Freimuth, F.; Blügel, S.; Mokrousov, Y. Crystal Hall and crystal magneto-optical effect in thin films of $SrRuO_3$. *J. Appl. Phys.* **2020**, *127*, 213904. [CrossRef]
21. Hayami, S.; Kusunose, H. Essential role of the anisotropic magnetic dipole in the anomalous Hall effect. *Phys. Rev. B* **2021**, *103*, L180407. [CrossRef]
22. Feng, Z.; Zhou, X.; Šmejkal, L.; Wu, L.; Zhu, Z.; Guo, H.; González-Hernández, R.; Wang, X.; Yan, H.; Qin, P.; et al. An anomalous Hall effect in altermagnetic ruthenium dioxide. *Nat. Electron.* **2022**, *5*, 735–743. [CrossRef]
23. Tomizawa, T.; Kontani, H. Anomalous Hall effect in the $t_{2g}$ orbital kagome lattice due to noncollinearity: Significance of the orbital Aharonov-Bohm effect. *Phys. Rev. B* **2009**, *80*, 100401. [CrossRef]
24. Chen, H.; Niu, Q.; MacDonald, A.H. Anomalous Hall Effect Arising from Noncollinear Antiferromagnetism. *Phys. Rev. Lett.* **2014**, *112*, 017205. [CrossRef]
25. Nakatsuji, S.; Kiyohara, N.; Higo, T. Large anomalous Hall effect in a non-collinear antiferromagnet at room temperature. *Nature* **2015**, *527*, 212. [CrossRef]
26. Suzuki, M.T.; Koretsune, T.; Ochi, M.; Arita, R. Cluster multipole theory for anomalous Hall effect in antiferromagnets. *Phys. Rev. B* **2017**, *95*, 094406. [CrossRef]
27. Chen, H.; Wang, T.C.; Xiao, D.; Guo, G.Y.; Niu, Q.; MacDonald, A.H. Manipulating anomalous Hall antiferromagnets with magnetic fields. *Phys. Rev. B* **2020**, *101*, 104418. [CrossRef]

28. Ohgushi, K.; Murakami, S.; Nagaosa, N. Spin anisotropy and quantum Hall effect in the *kagomé* lattice: Chiral spin state based on a ferromagnet. *Phys. Rev. B* **2000**, *62*, R6065–R6068. [CrossRef]
29. Shindou, R.; Nagaosa, N. Orbital Ferromagnetism and Anomalous Hall Effect in Antiferromagnets on the Distorted fcc Lattice. *Phys. Rev. Lett.* **2001**, *87*, 116801. [CrossRef]
30. Taguchi, Y.; Oohara, Y.; Yoshizawa, H.; Nagaosa, N.; Tokura, Y. Spin chirality, Berry phase, and anomalous Hall effect in a frustrated ferromagnet. *Science* **2001**, *291*, 2573–2576. [CrossRef]
31. Neubauer, A.; Pfleiderer, C.; Binz, B.; Rosch, A.; Ritz, R.; Niklowitz, P.G.; Böni, P. Topological Hall Effect in the *A* Phase of MnSi. *Phys. Rev. Lett.* **2009**, *102*, 186602. [CrossRef]
32. Hayami, S.; Kusunose, H. Unified description of electronic orderings and cross correlations by complete multipole representation. *J. Phys. Soc. Jpn.* **2024**, *93*, 072001. [CrossRef]
33. Kusunose, H.; Hayami, S. Generalization of microscopic multipoles and cross-correlated phenomena by their orderings. *J. Phys. Condense. Matter* **2022**, *34*, 464002. [CrossRef]
34. Suzuki, M.T.; Nomoto, T.; Arita, R.; Yanagi, Y.; Hayami, S.; Kusunose, H. Multipole expansion for magnetic structures: A generation scheme for a symmetry-adapted orthonormal basis set in the crystallographic point group. *Phys. Rev. B* **2019**, *99*, 174407. [CrossRef]
35. Kusunose, H.; Oiwa, R.; Hayami, S. Symmetry-adapted modeling for molecules and crystals. *Phys. Rev. B* **2023**, *107*, 195118. [CrossRef]
36. Yatsushiro, M.; Kusunose, H.; Hayami, S. Multipole classification in 122 magnetic point groups for unified understanding of multiferroic responses and transport phenomena. *Phys. Rev. B* **2021**, *104*, 054412. [CrossRef]
37. Hayami, S.; Kusunose, H. Microscopic Description of Electric and Magnetic Toroidal Multipoles in Hybrid Orbitals. *J. Phys. Soc. Jpn.* **2018**, *87*, 033709. [CrossRef]
38. Kusunose, H.; Oiwa, R.; Hayami, S. Complete Multipole Basis Set for Single-Centered Electron Systems. *J. Phys. Soc. Jpn.* **2020**, *89*, 104704. [CrossRef]
39. Hayami, S.; Yatsushiro, M.; Yanagi, Y.; Kusunose, H. Classification of atomic-scale multipoles under crystallographic point groups and application to linear response tensors. *Phys. Rev. B* **2018**, *98*, 165110. [CrossRef]
40. Winkler, R.; Zülicke, U. Theory of electric, magnetic, and toroidal polarizations in crystalline solids with applications to hexagonal lonsdaleite and cubic diamond. *Phys. Rev. B* **2023**, *107*, 155201. [CrossRef]
41. Gallego, S.V.; Perez-Mato, J.M.; Elcoro, L.; Tasci, E.S.; Hanson, R.M.; Momma, K.; Aroyo, M.I.; Madariaga, G. MAGNDATA: Towards a database of magnetic structures. I. The commensurate case. *J. Appl. Crystallogr.* **2016**, *49*, 1750–1776. [CrossRef]
42. Solana-Madruga, E.; Dos santos García, A.; Arévalo-López, A.; Ávila-Brande, D.; Ritter, C.; Attfield, J.; Sáez-Puche, R. High pressure synthesis of polar and non-polar cation-ordered polymorphs of $Mn_2ScSbO_6$. *Dalton Trans.* **2015**, *44*, 20441–20448. [CrossRef] [PubMed]
43. Rousse, G.; Rodríguez-Carvajal, J.; Wurm, C.; Masquelier, C. Spiral magnetic structure in the iron diarsenate $LiFeAs_2O_7$: A neutron diffraction study. *Phys. Rev. B* **2013**, *88*, 214433. [CrossRef]
44. Moron, M.C.; Palacio, F.; Rodríguez-Carvajal, J. Crystal and magnetic structures of RbMnF4 and KMnF4 investigated by neutron powder diffraction: The relationship between structure and magnetic properties in the Mn3+ layered perovskites $AMnF_4$ (A = Na, K, Rb, Cs). *J. Phys. Condens. Matter* **1993**, *5*, 4909. [CrossRef]
45. Damay, F.; Poienar, M.; Martin, C.; Maignan, A.; Rodriguez-Carvajal, J.; André, G.; Doumerc, J.P. Spin-lattice coupling induced phase transition in the $S = 2$ frustrated antiferromagnet $CuMnO_2$. *Phys. Rev. B* **2009**, *80*, 094410. [CrossRef]
46. Calder, S.; Haglund, A.V.; Kolesnikov, A.I.; Mandrus, D. Magnetic exchange interactions in the van der Waals layered antiferromagnet $MnPSe_3$. *Phys. Rev. B* **2021**, *103*, 024414. [CrossRef]
47. Rousse, G.; Rodríguez-Carvajal, J.; Wurm, C.; Masquelier, C. A neutron diffraction study of the antiferromagnetic diphosphate $LiFeP_2O_7$. *Solid State Sci.* **2002**, *4*, 973–978. [CrossRef]
48. Blasco, J.; García-Muñoz, J.L.; García, J.; Subías, G.; Stankiewicz, J.; Rodríguez-Velamazán, J.A.; Ritter, C. Magnetic order and magnetoelectric properties of $R_2CoMnO_6$ perovskites ($R$ = Ho, Tm, Yb, and Lu). *Phys. Rev. B* **2017**, *96*, 024409. [CrossRef]
49. Khalyavin, D.D.; Manuel, P.; Hatnean, M.C.; Petrenko, O.A. Fragile ground state and rigid field-induced structures in the zigzag ladder compound $BaDy_2O_4$. *Phys. Rev. B* **2021**, *103*, 134434. [CrossRef]
50. Solana-Madruga, E.; Ritter, C.; Aguilar-Maldonado, C.; Mentré, O.; Attfield, J.P.; Arévalo-López, Á.M. Mn 3 MnNb 2 O 9: High-pressure triple perovskite with 1: 2 B-site order and modulated spins. *Chem. Commun.* **2021**, *57*, 8441–8444. [CrossRef]
51. Ghara, S.; Suard, E.; Fauth, F.m.c.; Tran, T.T.; Halasyamani, P.S.; Iyo, A.; Rodríguez-Carvajal, J.; Sundaresan, A. Ordered aeschynite-type polar magnets $R$FeWO$_6$ ($R$ = Dy, Eu, Tb, and Y): A new family of type-II multiferroics. *Phys. Rev. B* **2017**, *95*, 224416. [CrossRef]
52. Li, M.R.; Adem, U.; McMitchell, S.R.; Xu, Z.; Thomas, C.I.; Warren, J.E.; Giap, D.V.; Niu, H.; Wan, X.; Palgrave, R.G.; et al. A polar corundum oxide displaying weak ferromagnetism at room temperature. *J. Am. Chem. Soc.* **2012**, *134*, 3737–3747. [CrossRef] [PubMed]
53. Favre, V.Y.; Tucker, G.S.; Ritter, C.; Sibille, R.; Manuel, P.; Frontzek, M.D.; Kriener, M.; Yang, L.; Berger, H.; Magrez, A.; et al. Ferrimagnetic 120° magnetic structure in $Cu_2OSO_4$. *Phys. Rev. B* **2020**, *102*, 094422. [CrossRef]

54. Herak, M.; Zorko, A.; Pregelj, M.; Zaharko, O.; Posnjak, G.; Jagličić, Z.; Potočnik, A.; Luetkens, H.; van Tol, J.; Ozarowski, A.; et al. Magnetic order and low-energy excitations in the quasi-one-dimensional antiferromagnet $CuSe_2O_5$ with staggered fields. *Phys. Rev. B* **2013**, *87*, 104413. [CrossRef]
55. Sala, G.; Stone, M.B.; Rai, B.K.; May, A.F.; Laurell, P.; Garlea, V.O.; Butch, N.P.; Lumsden, M.D.; Ehlers, G.; Pokharel, G.; et al. Van Hove singularity in the magnon spectrum of the antiferromagnetic quantum honeycomb lattice. *Nat. Commun.* **2021**, *12*, 171. [CrossRef]
56. Ji, W.H.; Yin, L.; Zhu, W.M.; Kumar, C.M.N.; Li, C.; Li, H.F.; Jin, W.T.; Nandi, S.; Sun, X.; Su, Y.; et al. Noncollinear magnetic structure and anisotropic magnetoelastic coupling in cobalt pyrovanadate $Co_2V_2O_7$. *Phys. Rev. B* **2019**, *100*, 134420. [CrossRef]
57. May, A.F.; Liu, Y.; Calder, S.; Parker, D.S.; Pandey, T.; Cakmak, E.; Cao, H.; Yan, J.; McGuire, M.A. Magnetic order and interactions in ferrimagnetic $Mn_3Si_2Te_6$. *Phys. Rev. B* **2017**, *95*, 174440. [CrossRef]
58. Rousse, G.; Rodriguez-Carvajal, J.; Patoux, S.; Masquelier, C. Magnetic structures of the triphylite $LiFePO_4$ and of its delithiated form $FePO_4$. *Chem. Mater.* **2003**, *15*, 4082–4090. [CrossRef]
59. Wawrzyńska, E.; Coldea, R.; Wheeler, E.M.; Sörgel, T.; Jansen, M.; Ibberson, R.M.; Radaelli, P.G.; Koza, M.M. Charge disproportionation and collinear magnetic order in the frustrated triangular antiferromagnet $AgNiO_2$. *Phys. Rev. B* **2008**, *77*, 094439. [CrossRef]
60. Lu, K.; Sapkota, D.; DeBeer-Schmitt, L.; Wu, Y.; Cao, H.B.; Mannella, N.; Mandrus, D.; Aczel, A.A.; MacDougall, G.J. Canted antiferromagnetic order in the monoaxial chiral magnets $V_{1/3}TaS_2$ and $V_{1/3}NbS_2$. *Phys. Rev. Mater.* **2020**, *4*, 054416. [CrossRef]
61. Gonzalo, J.A.; Cox, D.E.; Shirane, G. The Magnetic Structure of $FeSb_2O_4$. *Phys. Rev.* **1966**, *147*, 415–418. [CrossRef]
62. Rodríguez-Carvajal, J.; Rosenkranz, S.; Medarde, M.; Lacorre, P.; Fernandez-Díaz, M.T.; Fauth, F.; Trounov, V. Neutron-diffraction study of the magnetic and orbital ordering in $^{154}SmNiO_3$ and $^{153}EuNiO_3$. *Phys. Rev. B* **1998**, *57*, 456–464. [CrossRef]
63. Caignaert, V.; Pralong, V.; Hardy, V.; Ritter, C.; Raveau, B. Magnetic structure of $CaBaCo_4O_7$: Lifting of geometrical frustration towards ferrimagnetism. *Phys. Rev. B* **2010**, *81*, 094417. [CrossRef]
64. Gitgeatpong, G.; Zhao, Y.; Avdeev, M.; Piltz, R.O.; Sato, T.J.; Matan, K. Magnetic structure and Dzyaloshinskii-Moriya interaction in the $S = \frac{1}{2}$ helical-honeycomb antiferromagnet $\alpha$-$Cu_2V_2O_7$. *Phys. Rev. B* **2015**, *92*, 024423. [CrossRef]
65. Cockayne, E.; Levin, I.; Wu, H.; Llobet, A. Magnetic structure of bixbyite $\alpha$-$Mn_2O_3$: A combined DFT+$U$ and neutron diffraction study. *Phys. Rev. B* **2013**, *87*, 184413. [CrossRef]
66. Huang, Q.; Qiu, Y.; Bao, W.; Green, M.A.; Lynn, J.W.; Gasparovic, Y.C.; Wu, T.; Wu, G.; Chen, X.H. Neutron-Diffraction Measurements of Magnetic Order and a Structural Transition in the Parent $BaFe_2As_2$ Compound of FeAs-Based High-Temperature Superconductors. *Phys. Rev. Lett.* **2008**, *101*, 257003. [CrossRef]
67. Troć, R.; Pasturel, M.; Tougait, O.; Sazonov, A.P.; Gukasov, A.; Sułkowski, C.; Noël, H. Single-crystal study of the kagome antiferromagnet $U_3Ru_4Al_{12}$. *Phys. Rev. B* **2012**, *85*, 064412. [CrossRef]
68. Brown, P.; Forsyth, J. A neutron diffraction study of weak ferromagnetism in nickel fluoride. *J. Phys. C: Solid State Phys.* **1981**, *14*, 5171. [CrossRef]
69. Will, G.; Schäfer, W.; Pfeiffer, F.; Elf, F.; Etourneau, J. Neutron diffraction studies of TbB4 and ErB4. *J. Less-Common Met.* **1981**, *82*, 349–355. [CrossRef]
70. Podchezertsev, S.; Barrier, N.; Pautrat, A.; Suard, E.; Retuerto, M.; Alonso, J.A.; Fernandez-Diaz, M.T.; Rodríguez-Carvajal, J. Influence of Polymorphism on the Magnetic Properties of Co5TeO8 Spinel. *Inorg. Chem.* **2021**, *60*, 13990–14001. [CrossRef]
71. Adroja, D.T.; de la Fuente, C.; Fraile, A.; Hillier, A.D.; Daoud-Aladine, A.; Kockelmann, W.; Taylor, J.W.; Koza, M.M.; Burzurí, E.; Luis, F.; et al. Muon spin rotation and neutron scattering study of the noncentrosymmetric tetragonal compound $CeAuAl_3$. *Phys. Rev. B* **2015**, *91*, 134425. [CrossRef]
72. Lacorre, P.; Pannetier, J.; Fleischer, T.; Hoppe, R.; Ferey, G. Ordered magnetic frustration: XVI. Magnetic structure of $CsCoF_4$ at 1.5 K. *J. Solid State Chem.* **1991**, *93*, 37–45. [CrossRef]
73. Fruchart, D.; F. Bertaut, E. Magnetic studies of the metallic perovskite-type compounds of manganese. *J. Phys. Soc. Jpn.* **1978**, *44*, 781–791. [CrossRef]
74. Paul, A.K.; Reehuis, M.; Ksenofontov, V.; Yan, B.; Hoser, A.; Többens, D.M.; Abdala, P.M.; Adler, P.; Jansen, M.; Felser, C. Lattice Instability and Competing Spin Structures in the Double Perovskite Insulator $Sr_2FeOsO_6$. *Phys. Rev. Lett.* **2013**, *111*, 167205. [CrossRef]
75. May, A.F.; McGuire, M.A.; Cao, H.; Sergueev, I.; Cantoni, C.; Chakoumakos, B.C.; Parker, D.S.; Sales, B.C. Spin Reorientation in $TlFe_{1.6}Se_2$ with Complete Vacancy Ordering. *Phys. Rev. Lett.* **2012**, *109*, 077003. [CrossRef]
76. Injac, S.; Yuen, A.K.; Avdeev, M.; Orlandi, F.; Kennedy, B.J. Structural and magnetic studies of KOsO 4, a 5d 1 quantum magnet oxide. *Phys. Chem. Chem. Phys.* **2019**, *21*, 7261–7264. [CrossRef]
77. Morosan, E.; Fleitman, J.A.; Huang, Q.; Lynn, J.W.; Chen, Y.; Ke, X.; Dahlberg, M.L.; Schiffer, P.; Craley, C.R.; Cava, R.J. Structure and magnetic properties of the $Ho_2Ge_2O_7$ pyrogermanate. *Phys. Rev. B* **2008**, *77*, 224423. [CrossRef]
78. Babkevich, P.; Testa, L.; Kimura, K.; Kimura, T.; Tucker, G.S.; Roessli, B.; Rønnow, H.M. Magnetic structure of $Ba(TiO)Cu_4(PO_4)_4$ probed using spherical neutron polarimetry. *Phys. Rev. B* **2017**, *96*, 214436. [CrossRef]
79. Taddei, K.M.; Sanjeewa, L.; Kolis, J.W.; Sefat, A.S.; de la Cruz, C.; Pajerowski, D.M. Local-Ising-type magnetic order and metamagnetism in the rare-earth pyrogermanate $Er_2Ge_2O_7$. *Phys. Rev. Mater.* **2019**, *3*, 014405. [CrossRef]
80. Cadogan, J.; Ryan, D.; Altounian, Z.; Wang, H.; Swainson, I. The magnetic structures of $Nd_5Si_4$ and $Nd_5Ge_4$. *J. Phys. Condens. Matter* **2002**, *14*, 7191. [CrossRef]

81. Hillier, A.D.; Adroja, D.T.; Manuel, P.; Anand, V.K.; Taylor, J.W.; McEwen, K.A.; Rainford, B.D.; Koza, M.M. Muon spin relaxation and neutron scattering investigations of the noncentrosymmetric heavy-fermion antiferromagnet $CeRhGe_3$. *Phys. Rev. B* **2012**, *85*, 134405. [CrossRef]
82. Anand, V.K.; Hillier, A.D.; Adroja, D.T.; Khalyavin, D.D.; Manuel, P.; Andre, G.; Rols, S.; Koza, M.M. Understanding the magnetism in noncentrosymmetric $CeIrGe_3$: Muon spin relaxation and neutron scattering studies. *Phys. Rev. B* **2018**, *97*, 184422. [CrossRef]
83. Sale, M.; Xia, Q.; Avdeev, M.; Ling, C.D. Crystal and Magnetic Structures of Melilite-Type $Ba_2MnSi_2O_7$. *Inorg. Chem.* **2019**, *58*, 4164–4172. [CrossRef]
84. Zou, T.; Cai, Y.Q.; dela Cruz, C.R.; Garlea, V.O.; Mahanti, S.D.; Cheng, J.G.; Ke, X. Up-up-down-down magnetic chain structure of the spin-$\frac{1}{2}$ tetragonally distorted spinel $GeCu_2O_4$. *Phys. Rev. B* **2016**, *94*, 214406. [CrossRef]
85. Nirmala, R.; Morozkin, A.; Isnard, O.; Nigam, A. Understanding the magnetic ground state of rare-earth intermetallic compound Ce4Sb3: Magnetization and neutron diffraction studies. *J. Magn. Magn. Mater.* **2009**, *321*, 188–191. [CrossRef]
86. Nandi, S.; Xiao, Y.; Qureshi, N.; Paramanik, U.B.; Jin, W.T.; Su, Y.; Ouladdiaf, B.; Hossain, Z.; Brückel, T. Magnetic structures of the Eu and Cr moments in $\mathbf{EuCr_2As_2}$: Neutron diffraction study. *Phys. Rev. B* **2016**, *94*, 094411. [CrossRef]
87. Dalmas de Réotier, P.; Marin, C.; Yaouanc, A.; Ritter, C.; Maisuradze, A.; Roessli, B.; Bertin, A.; Baker, P.J.; Amato, A. Long-range dynamical magnetic order and spin tunneling in the cooperative paramagnetic states of the pyrochlore analogous spinel antiferromagnets $CdYb_2X_4$ ($X =$ S or Se). *Phys. Rev. B* **2017**, *96*, 134403. [CrossRef]
88. Hofmann, M.; Campbell, S.J.; Edge, A.V.J. $EuMn_2Ge_2$ and $EuMn_2Si_2$ : Magnetic structures and valence transitions. *Phys. Rev. B* **2004**, *69*, 174432. [CrossRef]
89. Cui, Q.; Huang, Q.; Alonso, J.A.; Sheptyakov, D.; De la Cruz, C.R.; Fernández-Díaz, M.T.; Wang, N.N.; Cai, Y.Q.; Li, D.; Dong, X.L.; et al. Complex antiferromagnetic order in the garnet $Co_3Al_2Si_3O_{12}$. *Phys. Rev. B* **2020**, *101*, 144424. [CrossRef]
90. Jauch, W.; Reehuis, M.; Schultz, A. $\gamma$-ray and neutron diffraction studies of $CoF_2$: Magnetostriction, electron density and magnetic moments. *Acta Crystallogr. A* **2004**, *60*, 51–57. [CrossRef]
91. Calder, S.; Saparov, B.; Cao, H.B.; Niedziela, J.L.; Lumsden, M.D.; Sefat, A.S.; Christianson, A.D. Magnetic structure and spin excitations in $BaMn_2Bi_2$. *Phys. Rev. B* **2014**, *89*, 064417. [CrossRef]
92. Wiebe, C.R.; Gardner, J.S.; Kim, S.J.; Luke, G.M.; Wills, A.S.; Gaulin, B.D.; Greedan, J.E.; Swainson, I.; Qiu, Y.; Jones, C.Y. Magnetic Ordering in the Spin-Ice Candidate $Ho_2Ru_2O_7$. *Phys. Rev. Lett.* **2004**, *93*, 076403. [CrossRef]
93. Blanco, J.A.; Brown, P.J.; Stunault, A.; Katsumata, K.; Iga, F.; Michimura, S. Magnetic structure of $GdB_4$ from spherical neutron polarimetry. *Phys. Rev. B* **2006**, *73*, 212411. [CrossRef]
94. Bos, J.W.G.; Colin, C.V.; Palstra, T.T.M. Magnetoelectric coupling in the cubic ferrimagnet $Cu_2OSeO_3$. *Phys. Rev. B* **2008**, *78*, 094416. [CrossRef]
95. Kenzelmann, M.; Lawes, G.; Harris, A.B.; Gasparovic, G.; Broholm, C.; Ramirez, A.P.; Jorge, G.A.; Jaime, M.; Park, S.; Huang, Q.; et al. Direct Transition from a Disordered to a Multiferroic Phase on a Triangular Lattice. *Phys. Rev. Lett.* **2007**, *98*, 267205. [CrossRef]
96. Volkova, O.S.; Mazurenko, V.V.; Solovyev, I.V.; Deeva, E.B.; Morozov, I.V.; Lin, J.Y.; Wen, C.K.; Chen, J.M.; Abdel-Hafiez, M.; Vasiliev, A.N. Noncollinear ferrimagnetic ground state in $Ni(NO_3)_2$. *Phys. Rev. B* **2014**, *90*, 134407. [CrossRef]
97. Saito, T.; Toyoda, M.; Ritter, C.; Zhang, S.; Oguchi, T.; Attfield, J.P.; Shimakawa, Y. Symmetry-breaking 60°-spin order in the A-site-ordered perovskite $LaMn_3V_4O_{12}$. *Phys. Rev. B* **2014**, *90*, 214405. [CrossRef]
98. Haraguchi, Y.; Nawa, K.; Michioka, C.; Ueda, H.; Matsuo, A.; Kindo, K.; Avdeev, M.; Sato, T.J.; Yoshimura, K. Frustrated magnetism in the $J_1 - J_2$ honeycomb lattice compounds $MgMnO_3$ and $ZnMnO_3$ synthesized via a metathesis reaction. *Phys. Rev. Mater.* **2019**, *3*, 124406. [CrossRef]
99. Li, F.; Pomjakushin, V.; Mazet, T.; Sibille, R.; Malaman, B.; Yadav, R.; Keller, L.; Medarde, M.; Conder, K.; Pomjakushina, E. Revisiting the magnetic structure and charge ordering in $La_{1/3}Sr_{2/3}FeO_3$ by neutron powder diffraction and Mössbauer spectroscopy. *Phys. Rev. B* **2018**, *97*, 174417. [CrossRef]
100. Ritter, C.; Pankrats, A.; Gudim, I.; Vorotynov, A. Magnetic structure of iron borate $DyFe_3(BO_3)_4$: A neutron diffraction study. *J. Phys. Conf. Ser.* **2012**, *340*, 012065. [CrossRef]
101. Boldrin, D.; Fåk, B.; Canévet, E.; Ollivier, J.; Walker, H.C.; Manuel, P.; Khalyavin, D.D.; Wills, A.S. Vesignieite: An $S = \frac{1}{2}$ Kagome Antiferromagnet with Dominant Third-Neighbor Exchange. *Phys. Rev. Lett.* **2018**, *121*, 107203. [CrossRef]
102. Hao, X.F.; Stroppa, A.; Picozzi, S.; Filippetti, A.; Franchini, C. Exceptionally large room-temperature ferroelectric polarization in the $PbNiO_3$ multiferroic nickelate: First-principles study. *Phys. Rev. B* **2012**, *86*, 014116. [CrossRef]
103. Hwang, J.; Choi, E.S.; Ye, F.; Dela Cruz, C.R.; Xin, Y.; Zhou, H.D.; Schlottmann, P. Successive Magnetic Phase Transitions and Multiferroicity in the Spin-One Triangular-Lattice Antiferromagnet $Ba_3NiNb_2O_9$. *Phys. Rev. Lett.* **2012**, *109*, 257205. [CrossRef]
104. Corliss, L.M.; Elliott, N.; Hastings, J.M.; Sass, R.L. Magnetic Structure of Chromium Selenide. *Phys. Rev.* **1961**, *122*, 1402–1406. [CrossRef]
105. Zvereva, E.A.; Raganyan, G.V.; Vasilchikova, T.M.; Nalbandyan, V.B.; Gafurov, D.A.; Vavilova, E.L.; Zakharov, K.V.; Koo, H.J.; Pomjakushin, V.Y.; Susloparova, A.E.; et al. Hidden magnetic order in the triangular-lattice magnet $Li_2MnTeO_6$. *Phys. Rev. B* **2020**, *102*, 094433. [CrossRef]
106. Tian, W.; Svoboda, C.; Ochi, M.; Matsuda, M.; Cao, H.B.; Cheng, J.G.; Sales, B.C.; Mandrus, D.G.; Arita, R.; Trivedi, N.; et al. High antiferromagnetic transition temperature of the honeycomb compound $SrRu_2O_6$. *Phys. Rev. B* **2015**, *92*, 100404. [CrossRef]

107. Milam-Guerrero, J.; Zheng, M.; Spence, N.R.; Falsaperna, M.; Calder, S.; Lapidus, S.; Saines, P.J.; Melot, B.C. Influence of the cubic sublattice on magnetic coupling between the tetrahedral sites of garnet. *Inorg. Chem.* **2021**, *60*, 8500. [CrossRef]
108. Kurbakov, A.I.; Susloparova, A.E.; Pomjakushin, V.Y.; Skourski, Y.; Vavilova, E.L.; Vasilchikova, T.M.; Raganyan, G.V.; Vasiliev, A.N. Commensurate helicoidal order in the triangular layered magnet $Na_2MnTeO_6$. *Phys. Rev. B* **2022**, *105*, 064416. [CrossRef]
109. Soh, J.R.; Yi, C.; Zivkovic, I.; Qureshi, N.; Stunault, A.; Ouladdiaf, B.; Rodríguez-Velamazán, J.A.; Shi, Y.; Rønnow, H.M.; Boothroyd, A.T. Magnetic structure of the topological semimetal $Co_3Sn_2S_2$. *Phys. Rev. B* **2022**, *105*, 094435. [CrossRef]
110. Ding, L.; Xu, X.; Jeschke, H.O.; Bai, X.; Feng, E.; Alemayehu, A.S.; Kim, J.; Huang, F.T.; Zhang, Q.; Ding, X.; et al. Field-tunable toroidal moment in a chiral-lattice magnet. *Nat. Commun.* **2021**, *12*, 5339. [CrossRef]
111. Brown, P.; Chatterji, T. Neutron diffraction and polarimetric study of the magnetic and crystal structures of $HoMnO_3$ and $YMnO_3$. *J. Phys. Condens. Matter* **2006**, *18*, 10085. [CrossRef]
112. Szytuła, A.; Penc, B.; Hernandez-Velasco, J.; Zygmunt, A. Magnetic structures of RTIn (R = Ce, Er; T = Au, Ni) compounds. *J. Magn. Magn. Mater.* **2003**, *262*, L177–L180. [CrossRef]
113. Pomjakushin, V.; Perez-Mato, J.M.; Fischer, P.; Keller, L.; Sikora, W. Revisiting the antiferromagnetic structure of Tb14Ag51: the importance of distinguishing alternative symmetries for a multidimensional order parameter. *Acta Cryst. B* **2022**, *78*. [CrossRef]
114. Leblanc, M.; De Pape, R.; Ferey, G.; Pannetier, J. Ordered magnetic frustration–V. Antiferromagnetic structure of the hexagonal bronzoid HTB $FeF_3$; Comparison with the non frustrated rhombohedral form. *Solid State Commun.* **1986**, *58*, 171–176. [CrossRef]
115. Garlea, V.O.; Sanjeewa, L.D.; McGuire, M.A.; Batista, C.D.; Samarakoon, A.M.; Graf, D.; Winn, B.; Ye, F.; Hoffmann, C.; Kolis, J.W. Exotic Magnetic Field-Induced Spin-Superstructures in a Mixed Honeycomb-Triangular Lattice System. *Phys. Rev. X* **2019**, *9*, 011038. [CrossRef]
116. Brown, P.; Crangle, J.; Neumann, K.U.; Smith, J.G.; Ziebeck, K. The structure and magnetic moment distribution in the antiferromagnetic phase of. *J. Phys. Condens. Matter* **1997**, *9*, 4729. [CrossRef]
117. Schobinger-Papamantellos, P.; Rodríguez-Carvajal, J.; Buschow, K. Magnetic ordering of ScMn6Ge6 by neutron diffraction. *J. Magn. Magn. Mater.* **2014**, *369*, 243–248. [CrossRef]
118. Riberolles, S.X.; Trevisan, T.V.; Kuthanazhi, B.; Heitmann, T.; Ye, F.; Johnston, D.; Bud'ko, S.; Ryan, D.; Canfield, P.; Kreyssig, A.; et al. Magnetic crystalline-symmetry-protected axion electrodynamics and field-tunable unpinned Dirac cones in $EuIn_2As_2$. *Nat. Commun.* **2021**, *12*, 999. [CrossRef]
119. Munoz, A.; Alonso, J.; Martínez-Lope, M.; Casáis, M.; Martínez, J.; Fernandez-Diaz, M. Evolution of the magnetic structure of hexagonal $HoMnO_3$ from neutron powder diffraction data. *Chem. Mater.* **2001**, *13*, 1497–1505. [CrossRef]
120. Tang, Y.S.; Wang, S.M.; Lin, L.; Li, C.; Zheng, S.H.; Li, C.F.; Zhang, J.H.; Yan, Z.B.; Jiang, X.P.; Liu, J.M. Collinear magnetic structure and multiferroicity in the polar magnet $Co_2Mo_3O_8$. *Phys. Rev. B* **2019**, *100*, 134112. [CrossRef]
121. Disseler, S.M.; Borchers, J.A.; Brooks, C.M.; Mundy, J.A.; Moyer, J.A.; Hillsberry, D.A.; Thies, E.L.; Tenne, D.A.; Heron, J.; Holtz, M.E.; et al. Magnetic Structure and Ordering of Multiferroic Hexagonal $LuFeO_3$. *Phys. Rev. Lett.* **2015**, *114*, 217602. [CrossRef] [PubMed]
122. Ma, J.; Kamiya, Y.; Hong, T.; Cao, H.B.; Ehlers, G.; Tian, W.; Batista, C.D.; Dun, Z.L.; Zhou, H.D.; Matsuda, M. Static and Dynamical Properties of the Spin-1/2 Equilateral Triangular-Lattice Antiferromagnet $Ba_3CoSb_2O_9$. *Phys. Rev. Lett.* **2016**, *116*, 087201. [CrossRef]
123. Hayashida, S.; Hagihala, M.; Avdeev, M.; Miura, Y.; Manaka, H.; Masuda, T. Magnetic order in the chemically substituted frustrated antiferromagnet $CsCrF_4$. *Phys. Rev. B* **2020**, *102*, 174440. [CrossRef]
124. Maletta, H.; Robinson, R.; Lawson, A.; Sechovskỳ, V.; Havela, L.; Jirman, L.; Divis, M.; Brück, E.; De Boer, F.; Andreev, A.; et al. On the magnetic structure of UNiGa. *J. Magn. Magn. Mater.* **1992**, *104*, 21–22. [CrossRef]
125. Hayashida, S.; Zaharko, O.; Kurita, N.; Tanaka, H.; Hagihala, M.; Soda, M.; Itoh, S.; Uwatoko, Y.; Masuda, T. Pressure-induced quantum phase transition in the quantum antiferromagnet $CsFeCl_3$. *Phys. Rev. B* **2018**, *97*, 140405. [CrossRef]
126. Baran, S.; Szytuła, A.; Kaczorowski, D.; Hernández-Velasco, J. Crystal and magnetic structures of RPdIn (R = Nd, Ho, Er) compounds. *J. Magn. Magn. Mater.* **2005**, *285*, 272–278. [CrossRef]
127. Watanabe, H.; Kunitomi, N. On the neutron diffraction study of FeGe. *J. Phys. Soc. Jpn.* **1966**, *21*, 1932–1935. [CrossRef]
128. Mekata, M.; Adachi, K. Magnetic structure of CsCoCl3. *J. Phys. Soc. Jpn.* **1978**, *44*, 806–812. [CrossRef]
129. May, A.F.; Calder, S.; Cantoni, C.; Cao, H.; McGuire, M.A. Magnetic structure and phase stability of the van der Waals bonded ferromagnet $Fe_{3-x}GeTe_2$. *Phys. Rev. B* **2016**, *93*, 014411. [CrossRef]
130. Eriksson, T.; Lizárraga, R.; Felton, S.; Bergqvist, L.; Andersson, Y.; Nordblad, P.; Eriksson, O. Crystal and magnetic structure of $Mn_3IrSi$. *Phys. Rev. B* **2004**, *69*, 054422. [CrossRef]
131. Pomjakushin, V.; Plokhikh, I.; White, J.S.; Fujishiro, Y.; Kanazawa, N.; Tokura, Y.; Pomjakushina, E. Topological magnetic structures in MnGe: Neutron diffraction and symmetry analysis. *Phys. Rev. B* **2023**, *107*, 024410. [CrossRef]
132. Yano, S.; Louca, D.; Yang, J.; Chatterjee, U.; Bugaris, D.E.; Chung, D.Y.; Peng, L.; Grayson, M.; Kanatzidis, M.G. Magnetic structure of $NiS_{2-x}Se_x$. *Phys. Rev. B* **2016**, *93*, 024409. [CrossRef]
133. Sato, T.J.; Ishikawa, A.; Sakurai, A.; Hattori, M.; Avdeev, M.; Tamura, R. Whirling spin order in the quasicrystal approximant $Au_{72}Al_{14}Tb_{14}$. *Phys. Rev. B* **2019**, *100*, 054417. [CrossRef]
134. Saeaun, P.; Zhao, Y.; Piyawongwatthana, P.; Sato, T.J.; Chou, F.C.; Avdeev, M.; Gitgeatpong, G.; Matan, K. Magnetic properties and magnetic structure of the frustrated quasi-one-dimensional antiferromagnet $SrCuTe_2O_6$. *Phys. Rev. B* **2020**, *102*, 134407. [CrossRef]

135. Samartzis, A.; Chillal, S.; Islam, A.T.M.N.; Siemensmeyer, K.; Prokes, K.; Voneshen, D.J.; Senyshyn, A.; Khalyavin, D.; Lake, B. Structural and magnetic properties of the quantum magnet $BaCuTe_2O_6$. *Phys. Rev. B* **2021**, *103*, 094417. [CrossRef]
136. Stewart, J.; Ehlers, G.; Wills, A.; Bramwell, S.T.; Gardner, J. Phase transitions, partial disorder and multi-k structures in $Gd_2Ti_2O_7$. *J. Phys. Condens. Matter* **2004**, *16*, L321. [CrossRef]
137. Fujii, H.; Uwatoko, Y.; Motoya, K.; Ito, Y.; Okamoto, T. Neutron diffraction and magnetic studies of CeZn and NdZn single crystals. *J. Magn. Magn. Mater.* **1987**, *63*, 114–116. [CrossRef]
138. Wawrzyńczak, R.; Tomasello, B.; Manuel, P.; Khalyavin, D.; Le, M.D.; Guidi, T.; Cervellino, A.; Ziman, T.; Boehm, M.; Nilsen, G.J.; et al. Magnetic order and single-ion anisotropy in $Tb_3Ga_5O_{12}$. *Phys. Rev. B* **2019**, *100*, 094442. [CrossRef]
139. Sodemann, I.; Fu, L. Quantum Nonlinear Hall Effect Induced by Berry Curvature Dipole in Time-Reversal Invariant Materials. *Phys. Rev. Lett.* **2015**, *115*, 216806. [CrossRef]
140. Spaldin, N.A.; Fechner, M.; Bousquet, E.; Balatsky, A.; Nordström, L. Monopole-based formalism for the diagonal magnetoelectric response. *Phys. Rev. B* **2013**, *88*, 094429. [CrossRef]
141. Khomskii, D. Magnetic monopoles and unusual dynamics of magnetoelectrics. *Nat. Commun.* **2014**, *5*, 4793. [CrossRef] [PubMed]
142. Thöle, F.; Fechner, M.; Spaldin, N.A. First-principles calculation of the bulk magnetoelectric monopole density: Berry phase and Wannier function approaches. *Phys. Rev. B* **2016**, *93*, 195167. [CrossRef]
143. Thöle, F.; Spaldin, N.A. Magnetoelectric multipoles in metals. *Philos. Trans. R. Soc. A* **2018**, *376*, 20170450. [CrossRef] [PubMed]
144. Misawa, R.; Arakawa, K.; Yoshioka, T.; Ueda, H.; Iga, F.; Tamasaku, K.; Tanaka, Y.; Kimura, T. Resonant X-ray diffraction study using circularly polarized X rays on antiferromagnetic $TbB_4$. *Phys. Rev. B* **2023**, *108*, 134433. [CrossRef]
145. Arakawa, K.; Hayashida, T.; Kimura, K.; Misawa, R.; Nagai, T.; Miyamoto, T.; Okamoto, H.; Iga, F.; Kimura, T. Detecting Magnetoelectric Effect in a Metallic Antiferromagnet via Nonreciprocal Rotation of Reflected Light. *Phys. Rev. Lett.* **2023**, *131*, 236702. [CrossRef] [PubMed]
146. Aizu, K. Possible species of ferroelectrics. *Phys. Rev.* **1966**, *146*, 423. [CrossRef]
147. Aizu, K. Possible species of "ferroelastic" crystals and of simultaneously ferroelectric and ferroelastic crystals. *J. Phys. Soc. Jpn.* **1969**, *27*, 387–396. [CrossRef]
148. Aizu, K. Possible species of ferromagnetic, ferroelectric, and ferroelastic crystals. *Phs. Rev. B* **1970**, *2*, 754. [CrossRef]
149. Nagaosa, N.; Sinova, J.; Onoda, S.; MacDonald, A.H.; Ong, N.P. Anomalous Hall effect. *Rev. Mod. Phys.* **2010**, *82*, 1539–1592. [CrossRef]
150. Xiao, D.; Chang, M.C.; Niu, Q. Berry phase effects on electronic properties. *Rev. Mod. Phys.* **2010**, *82*, 1959–2007. [CrossRef]
151. Ikhlas, M.; Tomita, T.; Koretsune, T.; Suzuki, M.T.; Nishio-Hamane, D.; Arita, R.; Otani, Y.; Nakatsuji, S. Large anomalous Nernst effect at room temperature in a chiral antiferromagnet. *Nat. Phys.* **2017**, *13*, 1085. [CrossRef]
152. Kuroda, K.; Tomita, T.; Suzuki, M.T.; Bareille, C.; Nugroho, A.; Goswami, P.; Ochi, M.; Ikhlas, M.; Nakayama, M.; Akebi, S.; et al. Evidence for magnetic Weyl fermions in a correlated metal. *Nat. Mater.* **2017**, *16*, 1090. [CrossRef] [PubMed]
153. Higo, T.; Man, H.; Gopman, D.B.; Wu, L.; Koretsune, T.; van't Erve, O.M.; Kabanov, Y.P.; Rees, D.; Li, Y.; Suzuki, M.T.; et al. Large magneto-optical Kerr effect and imaging of magnetic octupole domains in an antiferromagnetic metal. *Nat. Photonics* **2018**, *12*, 73. [CrossRef] [PubMed]
154. Chen, H. Electronic chiralization as an indicator of the anomalous Hall effect in unconventional magnetic systems. *Phys. Rev. B* **2022**, *106*, 024421. [CrossRef]
155. Yamasaki, Y.; Nakao, H.; Arima, T.h. Augmented Magnetic Octupole in Kagomé 120-degree Antiferromagnets Detectable via X-ray Magnetic Circular Dichroism. *J. Phys. Soc. Jpn.* **2020**, *89*, 083703. [CrossRef]
156. Hayami, S.; Kusunose, H.; Motome, Y. Spontaneous parity breaking in spin-orbital coupled systems. *Phys. Rev. B* **2014**, *90*, 081115. [CrossRef]
157. Hayami, S.; Kusunose, H.; Motome, Y. Emergent odd-parity multipoles and magnetoelectric effects on a diamond structure: Implication for the 5*d* transition metal oxides $A\mathrm{OsO}_4$ $(A = \mathrm{K, Rb, and\ Cs})$. *Phys. Rev. B* **2018**, *97*, 024414. [CrossRef]
158. Yanagi, Y.; Hayami, S.; Kusunose, H. Manipulating the magnetoelectric effect: Essence learned from $Co_4Nb_2O_9$. *Phys. Rev. B* **2018**, *97*, 020404. [CrossRef]
159. Dzyaloshinskii, I. On the magneto-electrical effect in antiferromagnets. *Sov. Phys. JETP* **1960**, *10*, 628–629.
160. Astrov, D. The magnetoelectric effect in antiferromagnetics. *Sov. Phys. JETP-USSR* **1960**, *11*, 708–709.
161. Astrov, D. Magnetoelectric effect in chromium oxide. *Sov. Phys. JETP* **1961**, *13*, 729–733.
162. Folen, V.J.; Rado, G.T.; Stalder, E.W. Anisotropy of the Magnetoelectric Effect in $Cr_2O_3$. *Phys. Rev. Lett.* **1961**, *6*, 607–608. [CrossRef]
163. Shitade, A.; Watanabe, H.; Yanase, Y. Theory of orbital magnetic quadrupole moment and magnetoelectric susceptibility. *Phys. Rev. B* **2018**, *98*, 020407(R). [CrossRef]
164. Watanabe, H.; Yanase, Y. Magnetic hexadecapole order and magnetopiezoelectric metal state in $\mathbf{Ba}_{1-x}\mathbf{K}_x\mathbf{Mn}_2\mathbf{As}_2$. *Phys. Rev. B* **2017**, *96*, 064432. [CrossRef]
165. Shiomi, Y.; Watanabe, H.; Masuda, H.; Takahashi, H.; Yanase, Y.; Ishiwata, S. Observation of a Magnetopiezoelectric Effect in the Antiferromagnetic Metal $EuMnBi_2$. *Phys. Rev. Lett.* **2019**, *122*, 127207. [CrossRef] [PubMed]
166. Hayami, S.; Kusunose, H. Spin-orbital-momentum locking under odd-parity magnetic quadrupole ordering. *Phys. Rev. B* **2021**, *104*, 045117. [CrossRef]

167. Wang, C.; Gao, Y.; Xiao, D. Intrinsic Nonlinear Hall Effect in Antiferromagnetic Tetragonal CuMnAs. *Phys. Rev. Lett.* **2021**, *127*, 277201. [CrossRef] [PubMed]
168. Liu, H.; Zhao, J.; Huang, Y.X.; Wu, W.; Sheng, X.L.; Xiao, C.; Yang, S.A. Intrinsic Second-Order Anomalous Hall Effect and Its Application in Compensated Antiferromagnets. *Phys. Rev. Lett.* **2021**, *127*, 277202. [CrossRef]
169. Kirikoshi, A.; Hayami, S. Microscopic mechanism for intrinsic nonlinear anomalous Hall conductivity in noncollinear antiferromagnetic metals. *Phys. Rev. B* **2023**, *107*, 155109. [CrossRef]
170. Yamaura, J.i.; Hiroi, Z. Crystal structure and magnetic properties of the 5$d$ transition metal oxides $A\mathrm{OsO}_4(A = \mathrm{K, Rb, Cs})$. *Phys. Rev. B* **2019**, *99*, 155113. [CrossRef]
171. Arima, T. Time-Reversal Symmetry Breaking and Consequent Physical Responses Induced by All-In-All-Out Type Magnetic Order on the Pyrochlore Lattice. *J. Phys. Soc. Jpn.* **2013**, *82*, 013705. [CrossRef]
172. Hayami, S.; Kusunose, H. Time-reversal switching responses in antiferromagnets. *Phys. Rev. B* **2023**, *108*, L140409. [CrossRef]
173. Xu, X.; Huang, F.T.; Cheong, S.W. Magnetic toroidicity. *J. Phys. Condens. Matter* **2024**, *36*, 203002. [CrossRef] [PubMed]
174. Hayashida, T.; Matsumoto, K.; Kimura, T. Electric-field-induced magnetic toroidal moment in a time-reversal-odd antiferromagnet. *arXiv* **2024**, arXiv:2406.03029.
175. Litvin, D.B. Ferroic classifications extended to ferrotoroidic crystals. *Acta Cryst. A* **2008**, *64*, 316–320. [CrossRef] [PubMed]
176. Popov, Y.F.; Kadomtseva, A.; Belov, D.; Vorob'ev, G.; Zvezdin, A. Magnetic-field-induced toroidal moment in the magnetoelectric $Cr_2O_3$. *J. Exp. Theor. Phys. Lett.* **1999**, *69*, 330–335. [CrossRef]
177. Schmid, H. On ferrotoroidics and electrotoroidic, magnetotoroidic and piezotoroidic effects. *Ferroelectrics* **2001**, *252*, 41–50. [CrossRef]
178. Ederer, C.; Spaldin, N.A. Towards a microscopic theory of toroidal moments in bulk periodic crystals. *Phys. Rev. B* **2007**, *76*, 214404. [CrossRef]
179. Spaldin, N.A.; Fiebig, M.; Mostovoy, M. The toroidal moment in condensed-matter physics and its relation to the magnetoelectric effect. *J. Phys. Condens. Matter* **2008**, *20*, 434203. [CrossRef]
180. Kopaev, Y.V. Toroidal ordering in crystals. *Physics-Uspekhi* **2009**, *52*, 1111–1125. [CrossRef]
181. Yanase, Y. Magneto-Electric Effect in Three-Dimensional Coupled Zigzag Chains. *J. Phys. Soc. Jpn.* **2014**, *83*, 014703. [CrossRef]
182. Hayami, S.; Kusunose, H.; Motome, Y. Toroidal order in metals without local inversion symmetry. *Phys. Rev. B* **2014**, *90*, 024432. [CrossRef]
183. Hayami, S.; Kusunose, H.; Motome, Y. Spontaneous Multipole Ordering by Local Parity Mixing. *J. Phys. Soc. Jpn.* **2015**, *84*, 064717. [CrossRef]
184. Hayami, S.; Kusunose, H.; Motome, Y. Emergent spin-valley-orbital physics by spontaneous parity breaking. *J. Phys. Condens. Matter* **2016**, *28*, 395601. [CrossRef]
185. Saito, H.; Uenishi, K.; Miura, N.; Tabata, C.; Hidaka, H.; Yanagisawa, T.; Amitsuka, H. Evidence of a New Current-Induced Magnetoelectric Effect in a Toroidal Magnetic Ordered State of $UNi_4B$. *J. Phys. Soc. Jpn.* **2018**, *87*, 033702. [CrossRef]
186. Kawaguchi, H.; Tatara, G. Effective Hamiltonian theory for nonreciprocal light propagation in magnetic Rashba conductor. *Phys. Rev. B* **2016**, *94*, 235148. [CrossRef]
187. Watanabe, H.; Yanase, Y. Nonlinear electric transport in odd-parity magnetic multipole systems: Application to Mn-based compounds. *Phys. Rev. Res.* **2020**, *2*, 043081. [CrossRef]
188. Watanabe, H.; Yanase, Y. Photocurrent response in parity-time symmetric current-ordered states. *Phys. Rev. B* **2021**, *104*, 024416. [CrossRef]
189. Suzuki, Y. Tunneling spin current in systems with spin degeneracy. *Phys. Rev. B* **2022**, *105*, 075201. [CrossRef]
190. Yatsushiro, M.; Oiwa, R.; Kusunose, H.; Hayami, S. Analysis of model-parameter dependences on the second-order nonlinear conductivity in $\mathcal{PT}$-symmetric collinear antiferromagnetic metals with magnetic toroidal moment on zigzag chains. *Phys. Rev. B* **2022**, *105*, 155157. [CrossRef]
191. Miyahara, S.; Furukawa, N. Nonreciprocal Directional Dichroism and Toroidalmagnons in Helical Magnets. *J. Phys. Soc. Jpn.* **2012**, *81*, 023712. [CrossRef]
192. Miyahara, S.; Furukawa, N. Theory of magneto-optical effects in helical multiferroic materials via toroidal magnon excitation. *Phys. Rev. B* **2014**, *89*, 195145. [CrossRef]
193. Hayami, S.; Kusunose, H.; Motome, Y. Asymmetric Magnon Excitation by Spontaneous Toroidal Ordering. *J. Phys. Soc. Jpn.* **2016**, *85*, 053705. [CrossRef]
194. Kondo, H.; Akagi, Y. Nonlinear magnon spin Nernst effect in antiferromagnets and strain-tunable pure spin current. *Phys. Rev. Res.* **2022**, *4*, 013186. [CrossRef]
195. Hayami, S.; Yatsushiro, M.; Kusunose, H. Nonlinear spin Hall effect in $\mathcal{PT}$-symmetric collinear magnets. *Phys. Rev. B* **2022**, *106*, 024405. [CrossRef]
196. Mook, A.; Neumann, R.R.; Johansson, A.; Henk, J.; Mertig, I. Origin of the magnetic spin Hall effect: Spin current vorticity in the Fermi sea. *Phys. Rev. Res.* **2020**, *2*, 023065. [CrossRef]
197. Hayami, S.; Yatsushiro, M. Spin Conductivity Based on Magnetic Toroidal Quadrupole Hidden in Antiferromagnets. *J. Phys. Soc. Jpn.* **2022**, *91*, 063702. [CrossRef]
198. Matsumoto, T.; Hayami, S. Nonreciprocal magnons due to symmetric anisotropic exchange interaction in honeycomb antiferromagnets. *Phys. Rev. B* **2020**, *101*, 224419. [CrossRef]

199. Hayami, S.; Yatsushiro, M. Nonlinear nonreciprocal transport in antiferromagnets free from spin-orbit coupling. *Phys. Rev. B* **2022**, *106*, 014420. [CrossRef]
200. Hayami, S.; Yatsushiro, M. Nonreciprocal Transport in Noncoplanar Magnetic Systems without Spin–Orbit Coupling, Net Scalar Chirality, or Magnetization. *J. Phys. Soc. Jpn.* **2022**, *91*, 094704. [CrossRef]
201. Kishine, J.i.; Kusunose, H.; Yamamoto, H.M. On the definition of chirality and enantioselective fields. *Isr. J. Chem.* **2022**, *62*, e202200049. [CrossRef]
202. Hayami, S.; Kusunose, H. Chiral charge as hidden order parameter in $URu_2Si_2$. *J. Phys. Soc. Jpn.* **2023**, *92*, 113704. [CrossRef]
203. Inda, A.; Oiwa, R.; Hayami, S.; Yamamoto, H.M.; Kusunose, H. Quantification of chirality based on electric toroidal monopole. *J. Chem. Phys.* **2024**, *160*, 184117. [CrossRef] [PubMed]
204. Yoda, T.; Yokoyama, T.; Murakami, S. Current-induced orbital and spin magnetizations in crystals with helical structure. *Sci. Rep.* **2015**, *5*, 12024. [CrossRef] [PubMed]
205. Furukawa, T.; Shimokawa, Y.; Kobayashi, K.; Itou, T. Observation of current-induced bulk magnetization in elemental tellurium. *Nat. Commun.* **2017**, *8*, 954. [CrossRef] [PubMed]
206. Furukawa, T.; Watanabe, Y.; Ogasawara, N.; Kobayashi, K.; Itou, T. Current-induced magnetization caused by crystal chirality in nonmagnetic elemental tellurium. *Phys. Rev. Res.* **2021**, *3*, 023111. [CrossRef]
207. Rikken, G.L.J.A.; Fölling, J.; Wyder, P. Electrical Magnetochiral Anisotropy. *Phys. Rev. Lett.* **2001**, *87*, 236602. [CrossRef] [PubMed]
208. Hlinka, J. Eight Types of Symmetrically Distinct Vectorlike Physical Quantities. *Phys. Rev. Lett.* **2014**, *113*, 165502. [CrossRef]
209. Hlinka, J.; Privratska, J.; Ondrejkovic, P.; Janovec, V. Symmetry Guide to Ferroaxial Transitions. *Phys. Rev. Lett.* **2016**, *116*, 177602. [CrossRef]
210. Jin, W.; Drueke, E.; Li, S.; Admasu, A.; Owen, R.; Day, M.; Sun, K.; Cheong, S.W.; Zhao, L. Observation of a ferro-rotational order coupled with second-order nonlinear optical fields. *Nat. Phys.* **2020**, *16*, 42–46. [CrossRef]
211. Cheong, S.W.; Lim, S.; Du, K.; Huang, F.T. Permutable SOS (symmetry operational similarity). *NPJ Quantum Mater.* **2021**, *6*, 58. [CrossRef]
212. Cheong, S.W.; Huang, F.T.; Kim, M. Linking emergent phenomena and broken symmetries through one-dimensional objects and their dot/cross products. *Rep. Prog. Phys.* **2022**, *85*, 124501. [CrossRef] [PubMed]
213. Hayashida, T.; Uemura, Y.; Kimura, K.; Matsuoka, S.; Hagihala, M.; Hirose, S.; Morioka, H.; Hasegawa, T.; Kimura, T. Phase transition and domain formation in ferroaxial crystals. *Phys. Rev. Mater.* **2021**, *5*, 124409. [CrossRef]
214. Hayashida, T.; Uemura, Y.; Kimura, K.; Matsuoka, S.; Morikawa, D.; Hirose, S.; Tsuda, K.; Hasegawa, T.; Kimura, T. Visualization of ferroaxial domains in an order-disorder type ferroaxial crystal. *Nat. Commun.* **2020**, *11*, 4582. [CrossRef] [PubMed]
215. Yokota, H.; Hayashida, T.; Kitahara, D.; Kimura, T. Three-dimensional imaging of ferroaxial domains using circularly polarized second harmonic generation microscopy. *NPJ Quantum Mater.* **2022**, *7*, 106. [CrossRef]
216. Fang, X.; De, C.; Huang, F.T.; Xu, X.; Du, K.; Wang, K.; Li, B.; Cheong, S.W. Ferrorotational Selectivity in Ilmenites. *J. Am. Chem. Soc.* **2023**, *145*, 28022–28029. [CrossRef]
217. Nasu, J.; Hayami, S. Antisymmetric thermopolarization by electric toroidicity. *Phys. Rev. B* **2022**, *105*, 245125. [CrossRef]
218. Roy, A.; Guimarães, M.H.D.; Sławińska, J. Unconventional spin Hall effects in nonmagnetic solids. *Phys. Rev. Mater.* **2022**, *6*, 045004. [CrossRef]
219. Hayami, S.; Oiwa, R.; Kusunose, H. Electric Ferro-Axial Moment as Nanometric Rotator and Source of Longitudinal Spin Current. *J. Phys. Soc. Jpn.* **2022**, *91*, 113702. [CrossRef]
220. Inda, A.; Hayami, S. Nonlinear Transverse Magnetic Susceptibility under Electric Toroidal Dipole Ordering. *J. Phys. Soc. Jpn.* **2023**, *92*, 043701. [CrossRef]
221. Kirikoshi, A.; Hayami, S. Rotational Response Induced by Electric Toroidal Dipole. *J. Phys. Soc. Jpn.* **2023**, *92*, 123703. [CrossRef]
222. Hayami, S. Ferroaxial moment induced by vortex spin texture. *Phys. Rev. B* **2022**, *106*, 144402. [CrossRef]
223. Inda, A.; Hayami, S. Magnetic instability under ferroaxial moment. *Phys. Rev. B* **2024**, *109*, 174424. [CrossRef]
224. Di Matteo, S.; Norman, M.R. Nature of the tensor order in $Cd_2Re_2O_7$. *Phys. Rev. B* **2017**, *96*, 115156. [CrossRef]
225. Hayami, S.; Yanagi, Y.; Kusunose, H.; Motome, Y. Electric Toroidal Quadrupoles in the Spin-Orbit-Coupled Metal $Cd_2Re_2O_7$. *Phys. Rev. Lett.* **2019**, *122*, 147602. [CrossRef] [PubMed]
226. Ishitobi, T.; Hattori, K. Magnetoelectric Effects and Charge-Imbalanced Solenoids: Antiferro Quadrupole Orders in a Diamond Structure. *J. Phys. Soc. Jpn.* **2019**, *88*, 063708. [CrossRef]
227. Göbel, B.; Mook, A.; Henk, J.; Mertig, I. Magnetoelectric effect and orbital magnetization in skyrmion crystals: Detection and characterization of skyrmions. *Phys. Rev. B* **2019**, *99*, 060406. [CrossRef]
228. Hayami, S.; Yambe, R. Helicity locking of a square skyrmion crystal in a centrosymmetric lattice system without vertical mirror symmetry. *Phys. Rev. B* **2022**, *105*, 104428. [CrossRef]
229. Bhowal, S.; Spaldin, N.A. Magnetoelectric Classification of Skyrmions. *Phys. Rev. Lett.* **2022**, *128*, 227204. [CrossRef]